Author Manuscript

Author Manuscript

Author Manuscript

Author Manuscript

HHS Public Access

Author manuscript

Nature. Author manuscript; available in PMC 2018 December 27.

Published in final edited form as:

Nature. 2018 July ; 559(7712): 130–134. doi:10.1038/s41586-018-0258-0.

The helicase Ded1p controls use of near-cognate translation initiation codons in 5′UTRs

Ulf-Peter Guenther[1,*], **David E. Weinberg**[2,3,*], **Meghan M. Zubradt**[2,4,*], **Frank A. Tedeschi**[1], **Brittany N. Stawicki**[1], **Leah L. Zagore**[1], **Gloria A. Brar**[5], **Donny D. Licatalosi**[1], **David P. Bartel**[3], **Jonathan S. Weissman**[2,4], and **Eckhard Jankowsky**[1,6,7]

[1]Center for RNA Science and Therapeutics, School of Medicine, Case Western Reserve University, Cleveland, OH 44106, USA

[2]Department of Cellular and Molecular Pharmacology, University of California, San Francisco, San Francisco, CA 94158, USA

[3]Howard Hughes Medical Institute; Whitehead Institute for Biomedical Research, 455 Main Street, Cambridge, MA 02142, USA; Department of Biology, Massachusetts Institute of Technology, Cambridge, MA 02139

[4]Howard Hughes Medical Institute and California Institute for Quantitative Biomedical Research, San Francisco, CA 94158, USA

[5]Department of Molecular and Cell Biology, University of California, Berkeley, CA 94720, USA

[6]Department of Physics, Case Western Reserve University, Cleveland, OH 44106, USA

Abstract

The conserved and essential DEAD-box RNA helicase Ded1p from yeast and its mammalian ortholog DDX3 are critical for translation initiation[1]. Mutations in DDX3 are linked to tumorigenesis[2–4] and intellectual disability[5], and the enzyme is targeted by diverse viruses[6]. How Ded1p and its orthologs engage RNAs in translation initiation has been a longstanding, unresolved question. Here we integrate transcriptome-wide analyses of RNA translation, structure, and Ded1p-RNA binding and show that the impact of Ded1p on translation initiation is connected to near-cognate initiation codons in 5′UTRs. Ded1p associates with the scanning translation pre-

Users may view, print, copy, and download text and data-mine the content in such documents, for the purposes of academic research, subject always to the full Conditions of use: http://www.nature.com/authors/editorial_policies/license.html#termsReprints and permission information is available at www.nature.com/reprints.

[7]Corresponding author. exj13@case.edu.
[*]These authors contributed equally
Correspondence and requests for materials should be addressed to E.J. (exj13@case.edu).

Supplementary Information is linked to the online version of the paper at www.nature.com/nature.

Author contributions

U.P.G: Conceptualization, material generation, ribosome profiling, xl-RAP-seq, iCLIP, mol. biol. techniques, bioinformatic analysis, statistical analysis, manuscript writing. D.E.W.: Conceptualization, iCLIP, M.M.Z.: Conceptualization, DMS-MaPSeq, bioinformatic analysis. F.A.T.: iCLIP, bioinformatic analysis, Western Blots. B.N.S.: Material generation, Northern Blots. L.L.Z., D.D.L.: iCLIP. G.A.B: Material generation meiosis strains, D.P.B.: Conceptualization, study supervision, J.S.W.: Conceptualization, study supervision. E.J.: Conceptualization, study supervision, manuscript writing. All authors commented on and edited the manuscript.

The authors declare no competing financial interests.

Readers are welcome to comment on the online version of the paper.

Author Manuscript Author Manuscript Author Manuscript Author Manuscript

initiation complex at the mRNA entry channel. Repression of Ded1p activity leads to accumulation of RNA structure in 5′UTRs, translation initiation from near-cognate start codons immediately upstream of these structures and decreased protein synthesis from the corresponding main ORFs. The data reveal a program for translation regulation that links Ded1p, activation of near-cognate start codons and mRNA structure. We show that this program plays a role in meiosis where a marked decrease in Ded1p levels is accompanied by activation of alternative translation initiation sites seen with repressed Ded1p activity. Our observations indicate that Ded1p impacts translation initiation by controlling the use of near-cognate initiation codons that are proximal to mRNA structure in 5′UTRs.

To systematically analyze how the essential Ded1p impacts translation initiation in cells, we first examined how a mutation in the enzyme altered the spectrum of ribosome footprints in cells[7]. We utilized the *ded1-95* mutation (Ded1p^{T408I}), which reduces affinity of Ded1p for RNA, diminishes RNA unwinding, and confers a temperature-sensitive growth defect to the budding yeast *S. cerevisiae*[8]. The mutation does not impact pre-mRNA splicing or ribosome biogenesis[9]. We performed ribosome profiling on wild type (WT) and *ded1-95* strains before and after temperature shift from 30°C to 37°C for 5 minutes (Extended data Fig. 1a–h). The short time was chosen to minimize effects on ribosome footprints arising from broad translation defects that are secondary to the direct impact of Ded1p.

At 30°C, WT and *ded1-95* strains showed virtually indistinguishable RNA expression and translation profiles (Extended data Fig. 1i,j). After the temperature shift, translation broadly decreased in *ded1-95*, compared to WT (Extended data Fig. 1k–n). These observations indicate that Ded1p promotes translation initiation for most mRNAs, consistent with previous findings[10,11]. However, translation of a subset of mRNAs coding for proteins involved in gluconeogenesis, cell wall synthesis and transcripts encoding histones were less affected by Ded1p than other mRNAs (Extended data Fig. 2a,b).

The fraction of ribosomes on 5′UTRs markedly increased upon temperature shift in *ded1-95*, compared to WT (Fig. 1a, Extended data Fig. 3a). The majority of mRNAs showed higher ribosome occupancy of the 5′UTR in *ded1-95*, which correlated with lower translation efficiency of the main open reading frame (ORF) (Fig. 1b, Extended data Fig. 3b). To examine the link between elevated ribosome occupancy in the 5′UTR and diminished translation of the main ORF, we performed polysome fractionation, followed by Northern Blot analysis of individual mRNAs. The *PSA1* mRNA, whose translation efficiency is markedly affected by Ded1p, showed a distinct shift from polysomes to monosomes in *ded1-95*, compared to WT upon temperature shift, but not at 30°C (Fig. 1c,d, Extended data Fig. 3c). *TDH2* mRNA, which is largely unaffected by Ded1p, did not show a comparable shift (Fig. 1c,d). Collectively, these observations suggest that increased ribosome occupancy on 5′UTRs correlates with binding of the mRNA to only a single ribosome. This notion is consistent with previous reports.[12] Ribosome profiling on only the 80S monosome fraction upon temperature shift also showed more footprints on 5′UTRs in *ded1-95*, compared to WT (Extended data Fig. 3d), indicating that ribosome occupancy on 5′UTRs broadly correlates with binding of mRNAs to single ribosomes.

Author Manuscript Author Manuscript Author Manuscript Author Manuscript

A large number of sites on 5′UTRs with increased ribosome footprints in *ded1-95* were enriched with near-cognate initiation codons (Fig. 1e–g), which differ from the canonical 5′-AUG-3′ initiation codon by a single nucleotide and can create alternative translation initiation sites (aTISs).[13] Increased ribosome occupancy on AUG codons in 5′UTRs was also seen in *ded1-95* (Fig. 1f), but only few of these sites exist in the yeast transcriptome, compared to nine different near-cognate initiation codons, which constitute roughly 14% of all codons.[14] Ribosomes translate from the *ded1-95*-activated aTISs, as demonstrated by ribosome profiles on small ORFs starting at these aTISs and finishing at the respective termination codons, by lack of ribosome accumulation at aTISs when translation was not arrested, and by the periodicity of ribosome footprints starting from aTISs (Extended data Fig. 3e–l). Collectively, the data indicate that defective Ded1p leads to aTIS activation in 5′UTRs, which decreases polysome formation on the main ORFs and thereby overall protein production. We conclude that Ded1p function suppresses use of aTISs.

While aTIS activation in *ded1-95* was extensive, only a subset of all near-cognate initiation codons was used. We detected no preferred length or register of the corresponding small ORFs relative to the main ORFs. However, in the aTISs, near-cognate codons from which translation initiation is most efficient were over-represented, while near-cognate codons from which translation initiation is least efficient were underrepresented[15,16] (Extended data Fig. 4a). These observations show that aTIS activation is influenced by inherent codon preferences of the pre-initiation complex (PIC), although these preferences do not fully explain the aTIS activation pattern (Extended data Fig. 4b–e).

To better understand this pattern, we examined whether remodeling of mRNA secondary structure by Ded1p is linked to aTIS activation. As an RNA helicase, Ded1p has been implicated in RNA structure remodeling[11,17], but it is not known which mRNA structures Ded1p alters in cells. To delineate cellular mRNA structures remodeled by Ded1p, we used DMS probing *in vivo*[18] and measured changes in mRNA structure in *ded1-95* and WT strains upon temperature shift. (Extended data Fig. 5a,b, ref.[8]). Unwinding of mRNA structure by Ded1p was most pronounced in 5′UTRs, compared to other mRNA regions (Fig. 2a, Extended data Fig. 5c). Strikingly, *ded1-95* activated aTISs were generally located 5′ of unwound RNA regions (Fig. 2b,c). Even near-cognate codons for which translation initiation is least efficient were activated, if located 5′ of mRNA structure (Fig. 2b). Our observations link the inability of *ded1-95* to resolve mRNA structure to aTIS activation, suggesting that Ded1p suppresses aTIS activation by unwinding mRNA structure.

To investigate how Ded1p physically accomplishes this function, we determined which cellular RNAs bound to WT Ded1p using high-throughput crosslinking-based approaches (xl-RAP-seq) and the iCLIP technique to map Ded1p-binding sites on these RNAs[19] (Extended data Fig. 6a–c). Ded1p crosslinked predominantly to mRNAs and ribosomal RNA (Extended data Fig. 6b), especially to the 40S ribosomal subunit (Fig. 3a), which as part of the PIC scans 5′UTRs.[20] The most frequently crosslinked position maps to Helix 16, located at the mRNA entry channel (Fig. 3a). Notable crosslinking was also observed at Helix 26, located at the mRNA exit site, and in the Extension segment 6, around nucleotide 720, which is located in the vicinity of the other crosslink sites on the solvent side of the 40S subunit (Fig. 3a). Ded1p binding to Helices16 and 26 is consistent with reported interactions

Author Manuscript Author Manuscript Author Manuscript Author Manuscript

between Ded1p and eIF3c and the eIF3b/g/i sub-complex, that bind near these sites (Extended data Fig. 7a,b).[21,22] Human DDX3X also binds to Helix16.[3]

Ded1p further crosslinked to virtually all expressed mRNAs, predominantly in 5′UTRs (Fig. 3b,c). This crosslinking pattern is consistent with the physical link of Ded1p to the PIC. Aside from a modest preference for A and U, no sequence motifs could be identified in the mRNA crosslinking sites (Extended data Fig. 7c). However, peaks of Ded1p crosslinking on 5′UTRs were frequently proximal to *ded1-95* activated aTISs (Fig. 3c,d), and unwound mRNA structure was located 3′ of Ded1p crosslinking sites (Fig. 3c,f).

Collectively, the data link Ded1p binding to mRNA, unwound mRNA structure, aTIS location and binding of Ded1p to the PIC. This link is best illustrated by an example, here a segment of the *PSA1* mRNA (Fig. 4a). Ded1p binding is most pronounced 5′ of unwound RNA structure, indicating that Ded1p does not exclusively contact mRNA structure, but also regions 5′ of the structure. This finding is consistent with the notion that Ded1p functions in the context of the scanning PIC. The scanning process is slowed by RNA structure[20,23], and a slowed PIC conceivably permits Ded1p to survey the mRNA for structured regions that it then unwinds. Biochemical data show higher functional affinity of Ded1p for unstructured, compared to structured RNA[8], rationalizing the contacts of Ded1p to unpaired mRNA 5′ of unwound mRNA structure, as the helicase travels 5′ to 3′ with the PIC.

Our data collectively indicate that failure of Ded1p to resolve mRNA structure leads to aTIS activation. To directly probe the link between mRNA unwinding and aTIS activation, we generated a *PSA1* mRNA with a mutation in an activated aTIS 5′ of unwound RNA structure. (Fig. 4b). The mutation markedly diminished the sensitivity to Ded1p-deficiency seen with the native *PSA1* mRNA (Fig. 4b,c). Alterations in the RNA structure 3′ of the aTIS also decreased sensitivity to Ded1p (Extended data Fig. 8a,b). Identical observations were made for mutations in an aTIS and the corresponding RNA structure in the *ATP5* mRNA (Extended data Fig. 8c–f). These results show that the impact of Ded1p on translation initiation depends not only on RNA unwinding, but also on proximal aTISs. Without a proximal aTIS, failure of Ded1p to unwind 5′UTR structures does not abrogate scanning of the PIC and subsequent translation of the main ORF (Extended data Fig. 9). This finding challenges the notion that cellular 5′UTR structures alone are insurmountable hindrances for the scanning PIC.

Together, our results suggest the following function of Ded1p on 5′UTRs (Fig. 4d). The enzyme associates with the PIC in the vicinity of the mRNA entry site of the small ribosomal subunit (Fig. 3a). This site is in close proximity to eIF4G and eIF4A (Extended data Fig. 7b), both of which bind Ded1p with high affinity and might therefore be important for recruitment and function of Ded1p on the PIC.[8,24,25] The density of Ded1p crosslinking sites on 5′UTRs increases with distance from the 5′-cap (Fig. 3b), suggesting gradual recruitment of Ded1p to the mRNA entry site during the scanning process. This notion is consistent with the reported increase of Ded1p function with greater distance from the 5′-cap and with 5′UTR length[11]. The mRNA binding pattern of Ded1p further suggests that Ded1p is targeted to its sites of action through association with the scanning PIC. This is an effective way to deploy the enzyme exactly at sites where it is needed, even though these

Author Manuscript Author Manuscript Author Manuscript Author Manuscript

sites lack common sequence or defined structure signatures. If Ded1p is missing or defective, mRNA structure persists, the PIC stalls and either dissociates from the mRNA, continues slowed scanning through the structure, or undergoes subunit joining and translation initiation if a near-cognate codon is present (Fig. 4d). Ribosomes initiating on an aTIS block subsequent scanning ribosomes from reaching the canonical initiation site, thereby decreasing translation efficiency for the main ORF (Fig. 1b). Unless an aTIS marks an N-terminal extension of the main ORF, PICs initiating at an aTIS are likely to be deterred from translating the main ORF. PICs encountering 5′UTR structures without proximal aTIS also interfere with scanning, but the kinetic pause introduced by PIC stalling, slowed scanning through the structure, or a combination of thereof, is shorter than on an activated aTIS. Slowed PICs will eventually reach the main ORF (Extended data Fig. 9), and therefore, 5′UTR structure alone impacts main ORF translation markedly less than in combination with proximal aTISs. Our model for Ded1p function does not preclude additional roles of the enzyme before the PIC scanning process[25]. However, the Ded1p function outlined above largely accounts for the observed Ded1p interactions with mRNA, and therefore, additional roles of Ded1p are likely restricted to transient Ded1p - mRNA interactions.

Finally, our data reveal a straightforward mechanism for activation of upstream ORFs. The mRNA structures in the 5′UTRs represent a large set of riboswitches that are sensitive to Ded1p. Active Ded1p turns the switches “off”, suppresses aTIS activation and allows efficient translation of the main ORF. Inactivation of the helicase, either by post-translational modifications[1], by metabolites such as AMP[26], by decreased Ded1p levels, or by sequestration of Ded1p in RNP granules[25,27] turns the switches “on”, activating the aTISs and thereby inhibiting translation from the corresponding main ORFs. Certain peptides translated from activated aTISs might also have direct biological functions[28], but the regulation described here appears independent of functional peptides.

This mechanism for activation of upstream ORFs is likely utilized in biological processes. This notion is supported by several lines of evidence. First, there is a marked increase in sequence conservation in the RNA regions around activated aTIS (Extended data Fig. 10a). Second, the *ded1-95* activated aTIS in the *ALA1* transcript produces an N-terminal extension that targets Ala1p to the mitochondria[29] (Extended data Fig. 10b). Third, during meiosis, aTIS activation[15] occurs in a pattern highly similar to the aTIS activation pattern seen with *ded1-95* upon temperature shift (Fig. 4e,f, Extended data Fig. 10c). Strikingly, we find markedly reduced Ded1p levels during meiosis (Fig. 4g, Extended data Fig. 10d). This link between Ded1p levels and activation of aTISs proximal to 5′UTR structures during meiosis suggests a role of Ded1p levels in this process. Collectively, our observations show that the regulatory program linking Ded1p to mRNA structure and aTIS activation is used in a physiological cellular process. The results indicate that intricate translation control and activation of upstream ORFs can be based on simple, ubiquitous elements: a helicase, mRNA structure and near-cognate initiation codons.

Author Manuscript Author Manuscript Author Manuscript Author Manuscript

MATERIALS AND METHODS

Materials

Yeast strains, Plasmids and Oligonucleotides—Yeast strains used in this study are listed in Supplementary Information Table S1. Strains were grown at 30°C unless stated otherwise. Primers, Northern blot probes and other DNA oligonucleotides are listed in Supplementary Information Table S2, RNA oligonucleotides are listed in Supplementary Information Table S3, DNA plasmids are listed in Supplementary Information Table S4.

Generation of yeast strain expressing Ded1p-HTBH—Construction of plasmid pEJ21 containing the N-terminally HA-tagged Ded1p was described previously[24]. pEJ21was then used to generate the plasmid pEJ5. The HA-tag was replaced by a sequence containing aHpaI and a SphI site (amplification with primers X1 and X2), generating pEJ1. The HTB-tag was amplified from pFA6-HTB-kanMX6 plasmid (gift by Peter Kaiser, UC Irvine, CA, USA) with primers X3 and X4. The resultant PCR product was cloned into pEJ1 via its HpaI and SphI sites yielding pEJ2. A second His_6-Tag was introduced by site-directed mutagenesis with primers X5 and X6 generating pEJ3. The C-terminal HTBH-Tag was introduced into pEJ4[24] by amplification of pEJ3 with primers X8 and X9 and subcloning with PflMI and SpeI into pEJ4, yielding pEJ5. pEJ5 was linearized and used to transform BY4741 by standard lithium acetate transformation yielding yeast strain yEJ2.

Generation of yeast strain expressing Ded1p-His_6FLAG_3—Yeast strain yDPB740, containing a C-terminal His_6FLAG_3 tag on the endogenous *DED1* allele, was generated from BY4742 using standard methods. Briefly, a homologous recombination template was designed comprising the 40 nucleotides upstream and downstream of the DED1 stop codon flanking the His_6FLAG_3 tag (with stop codon) and kanMX6 drug resistance cassette. This template was generated by amplifying from pFA6a-6xHis-3xFLAG-kanMX6 plasmid with primers DW1 and DW2. PCR product was used to transform BY4742 by standard lithium acetate transformation yielding yeast strain yDPB740.

Generation of yeast strain expressing WT, −Δ2° and −ΔaTIS PSA1 and ATP5 mRNAs—FLAG-tagged PSA1 and ATP5 strains were generated from the respective cDNAsusing standard methods as described above (pEJ14, pEJ15 and pEJ18, pEJ19, respectively). The FLAG-tag was appendedat the 3′ terminus of the PSA1 and ATP5 ORF, respectively. For PSA1, mutations in the aTIS in the 5′UTR(PSA1-ΔaTIS, pEJ16, Fig. 4b,c) contained the following changes: (c.-51A>C, c.-49A>C, c.-45T>A). Mutations in the 5′UTR mRNA structure (PSA1-Δ2°, pEJ17, Extended data Fig. 8a,b), contained the following changes: (c.-39_- 38AG>TC, c.-36_-35TA>AT, c.-32A>T,c.-24_-22AAA>TCT, c.-19_-18AA>CT). For ATP5, mutations in the aTIS in the 5′UTR (ATP5-ΔaTIS, pEJ20, Extended data Fig. 8e,f) contained the following changes: (c.-126A>C, c.-120_119TT>CC, c.-109A>C). Mutations in the 5′UTR mRNA structure (PSA1-Δ2°, pEJ22, Extended data Fig. 8e,f), contained the following changes: (c.-102C>A, c.-99C>A, c.-96G>A, c.-83G>A, c.-81C>A, c.-76G>A, c.-74G>A).

Author Manuscript Author Manuscript Author Manuscript Author Manuscript

Methods

Polysome analysis—Polysome analysis using 20U (A_{260}) lysate was performed as described[31], with a lower final concentration of cycloheximide (50 μg/ml). Briefly, following centrifugation through a 15 – 45 % (w/v) sucrose gradient, sixteen fractions were collected at a pump speed of S = 0.9 ml/min. RNA in each fraction was precipitated by adding 2 volumes of ice-cold ethanol incubating overnight at −80°C. RNA was extracted with phenol-chloroform according to standard protocols. Samples were applied to an 1.4 % agarose gel containing 6 % (v/v) formaldehyde, and electrophoresis was performed as described [31]. RNA was visualized with EtBr. The amount of 18S rRNA in each fraction of the gradient was quantified with ImageQuant 5.2 software (Molecular Dynamics).

Northern blot analysis—For ribosome association of individual mRNAs, gel electrophoresis following polysome analysis and fractionation was performed as described above. RNA was subsequently transferred to nitrocellulose membranes (AmershamHybond™–N, GE Healthcare) and further processed as described [31]. DNA oligonucleotides (Supplementary Information Table S2 [X85, X96, X105, X114]) were radiolabeled with PNK according to standard procedures. Probes were incubated with the membranes in hybridization buffer (6 × SSC, 0.1% SDS, 10 × Denhardt's reagent) overnight at 42°C. Membranes were subsequently washed three times with wash buffer (6 × SSC, 0.1% SDS). Probe signals were visualized by a Molecular Dynamics Phosphorimager (GE Healthcare) and quantified by ImageQuant 5.2 software (Molecular Dynamics). Normalized signal intensities were compiled for fractions corresponding to monosomes, light and heavy polysomes and averaged from at least three biological replicates.

Western blot analysis—Lysates from yeast strain A14201 at vegetative phase and stage 11 (ndt80 release timecourse) were prepared as described.[15] After loading equal amounts of protein on a 10% NEXT gel, denaturing gel electrophoresisand transfer to a PVDF membrane, Western blotting was performedwith anti-Ded1p (Rabbit; 1:5000) and anti-Hexokinase(Rabbit;1:10,000; US Biological) antibodies. Chemiluminescencewas quantified by Imagequant software. Hexokinaseserved as a loading control for normalization.

Ribosome profiling—Yeast cultures (500 ml) were grown at 30°C in rich media to mid-log phase (OD_{600} ~ 0.4) and divided into two equal volumes. Cycloheximide (final concentration, 50μg/ml) was added to one sample. Cells were rapidly harvested by centrifugation at 4,000 g for 2 min, and snap-frozen on dry ice. One volume of pre-warmed media (44°C) was added to the remaining sample, resulting in a temperature of 37°C for the entire volume. The temperature of 37°C was verified. The entire sample was immediately moved to a shaking incubator at 37°C. Five minutes after temperature shift, the yeast culture was treated with cycloheximide and cells were harvested as mentioned above. For run-off experiments, yeast cells were harvested in the absence of cycloheximide (Extended data Fig. 3e).

Cell lysis, RNase I treatment (Ambion) and sucrose gradient centrifugation was performed as described[32] for 25 units A_{260} per sample. In addition, lysates (~ 150 μl) were treated with 3.25 μl Turbo DNase I for 1h at 25°C. Purification and processing of ribosome-protected

Author Manuscript Author Manuscript Author Manuscript Author Manuscript

fragments were carried out as described [32], except that rRNA depletion with the RiboZero kit (Illumina) was omitted. Depletion of rRNA was performed at the level of circularized cDNA, as described [7] (1μl of a 5 μM mix of biotinylated DNA oligonucleotides, Supplementary Information Table S2 (X66–X80) and MyOne Streptavidin C1 DynaBeads (Invitrogen)). PCR amplification and sequencing was performed as described[7].

Monosome-protected fragments were isolated as described.[12] Briefly, sucrose gradient centrifugation of lysates was performed and fractions corresponding to monosomes were pooled and treated with 1/10 U RNase I per unit A_{260} lysate and 0.4U Turbo DNase I per unit A_{260} lysate for 1 h at 25 °C. Reactions were stopped by phenol-chloroform extraction of RNA. Monosome-protected fragments were processed as ribosome-protected fragments.

The fragmented mRNA control libraries were generated as described.[32] Sizing, concentration and quality of each DNA library was assessed with the High Sensitivity DNA kit on an Agilent2100 Bioanalyzer system. Up to eight DNA libraries were pooled before performing 50 bp single end read sequencing on an Illumina HiSeq2500 V2 in rapid run mode.

Processing of ribosome profiling data was performed as described.[32] Briefly, adaptor sequences and ribosomal reads were removed. Remaining reads were mapped to the sacCer3 genome with the TopHat software (parameters set as: --no-novel-juncs -N 2 --read-edit-dist 2 -- max-insertion-length 3 --max-deletion-length 3 -g 2. (www.yeastgenome.org)). All other parameters were kept at default settings.[33] The abundance of mRNAs in ribosome or monosome-protected fragments as well as in the fragmented RNA control libraries were determined using Cufflinks software.[33] These values were used to calculate translational efficiencies as described.[14] For the calculation of $\log_2$ ΔTE values we also included a constant factor reflecting the change in overall size of the mRNA pool, derived from spike-in RNA controls (Supplementary Information Table S3).

P-sites in ribosome-protected fragments (RPFs) were determined using the13th position from the 5′ end of reads with 28 or 29 nt.[14] The fraction of ribosomes on 5′UTRs was calculated for each mRNA by counting all RPFs on the 5′UTR (excluding positions −3 to −1), divided by the number of all RPFs mapped to the entire mRNA. mRNAs with 5′UTRs containing fewer than 10 nt were excluded from the analysis. The center of ribosome density (CRD) was calculated as described.[34] The shift in the CRD (ΔCRD) in *ded1-95* compared to WT *DED1* upon temperature shift was defined relative to the entire length of the mRNA according to:

$$\Delta\mathrm{CRD} = [(\mathrm{CRD}\,ded1-95) - (\mathrm{CRD\,WT}\,DED1)]/\,\mathrm{mRNA\,length}$$

A negative ΔCRD value marks increased ribosome accumulation in the 5′UTR in *ded1-95*.

Alternative Translation Initiation Sites (aTIS) were identified according to a previously described algorithm.[15] Briefly, a position is considered an aTIS, if (*i*) minimal ribosome count value (±1nt of the nucleotide under consideration) is greater than 9 (high stringency aTIS) or 4 (medium stringency aTIS) in all replicates; if (*ii*) the ratio of ribosome occupancy

Author Manuscript Author Manuscript Author Manuscript Author Manuscript

between two neighboring nucleotides 5′ to 3′ (pos^{n-1}/pos^{n}) is greater than or equal to 3 (high stringency aTIS) in all replicates, or greater or equal of 3 in one and greater than or equal to 1.75 in the other replicate (medium stringency aTIS); and if (*iii*) the normalized ribosome count in *ded1-95* cells 5′ after temperature shift to 37°C is 1.5 fold higher that in WT *DED1* in all replicates. This algorithm identified 396 high stringency aTIS and 2,126 medium stringency aTIS. Near-cognate codons were identified in 259 high stringency aTIS (65%) and 1,382 medium stringency aTIS (65%) within a moving window of ± 1nt. Canonical AUG initiation codons were found in 4% high stringency aTIS, and in 3% medium stringency aTIS. As control set, we collected all near-cognate codons on 5′UTRs of mRNA genes with a 5′UTR length between 20 and 500 nt. After removal of near-cognate codons in medium stringency aTIS, we identified 60,666 near cognate codons.

Cross-linking aided RNA affinity precipitation (xl-RAP-seq)—Yeast cells containing HTBH-tagged *DED1* were grown in rich media to an OD_{600} of 1.0 – 1.5, harvested by brief centrifugation at 4,000 g, re-suspended in ice-cold water or remaining YPD media, transferred to a Petridish, and subjected to UV-light in a Stratalinker (600 mJ/cm^2, 254 nm) on ice. Cells were washed in ice-cold water, sedimented by centrifugation for 5 min at 5,250 g, frozen on dry ice and stored at −80°C.

Frozen cells were lysed in QIA-1M buffer (100 mMNaH_2PO_4 pH 8, 10 mM Tris, 1M NaCl, 8 M Urea, 10 mM imidazole, 0.5% (w/v) IGEPAL, 2.5 mM beta-mercaptoethanol, 1 mM PMSF, proteaseinhibitor cocktail [Roche]) with glass beads six times for 30 s in a Beadbeater system (Biospec products). Glass beads were removed, and lysates were centrifuged at 5,250g for 30 min. Cleared lysates were incubated with Ni^{2+}-Agarose (40 µl slurry per g dry pellet weight, pre- equilibrated in buffer QIA-1M; Qiagen) overnight at 4°C. Ni^{2+}-beads were washed in 25 ml of wash buffer 1 (0.3 M NaCl, 10 mM Tris, 100 mM NaH_2PO_4, 8 M Urea, 10 mM imidazole) and sample was eluted with 10 ml elution buffer1 (0.3 M NaCl, 100 mM Tris, 50 mM NaH_2PO_4, 8 M Urea, 500 mM imidazole, 10% (v/v) glycerol). Eluates were then incubated with12.5 µl equilibrated Streptavidin-conjugated agarose resin (Pierce Technologies) per g dry pellet weight overnight at 4°C. Streptavidin beads were washed with 12.5 ml wash buffer 2 (0.3 M NaCl, 100 mM Tris, 8 M Urea, 0.5 mM EDTA) – containing 2% SDS, with wash buffer 2 (12.5 ml) without SDS, and with 1 × TEV buffer. Beads were next incubated with 50 U AcTEV (Invitrogen) for 2 h at 4°C. The sample was eluted with 2 × 0.9 ml TEV elution buffer (300 mMNaOAc, pH 6, 8 M Urea, 0.5% NP-40). Eluates were incubated with 175 µl Proteinase K (4 mg/ml; Roche), and the reaction was stopped by standard phenol/chloroform extraction. Released RNA was precipitated by ethanol precipitation overnight. RNA was re-suspended in 1 x Turbo DNAse buffer and incubated with 0.4 µl TurboDNAse (Ambion) in a final volume of 20 µl for 20 min at 37°C. Turbo DNAsewas inactivated according to the manufacturer's instruction and the RNA precipitated with ethanol.

cDNA was generated from the RNA sample using the "template switch" activity of M-MLV reverse transcriptase.[35] Reactions were performed in 20 µl according to the instructions of the manufacturer mix (Invitrogen) with 0.5 µl Superscript II and 0.05 µM final concentration of tailed random hexamer primer (X13, Supplementary Information Table S2). Reaction conditions were as follows:

Author Manuscript Author Manuscript Author Manuscript Author Manuscript

20°C: 10 min; 37°C: 10 min, 42°C: 45 min. Next, 0.25 μM of primers (X14 – X17, Supplementary Information Table S2) containing a 7 nt index and three guanosine ribonucleotides at their 3′ end were added to the reaction mix and reactions were performed at 42°C for 30 min. 4 μl of the resultant cDNA were used as template for amplification with primers X18 and X19 (Supplementary Information Table S2) and Advantage 2 polymerase mix (Clontech) for 30 cycles, according to the manufacturer's instructions. PCR products were precipitated and washed with 75 % ethanol. DNA libraries were sequenced as 36 bp single end reads on an Illumina Genome Analyzer. Reads were mapped to sacCer2 genome with bowtie software with default settings.

Reads were excluded from further analysis if their location was outside of the boundaries of a mRNA or other transcribed regions of the genome as previously defined.[36] Genes were only considered to be bound by Ded1p, if more than 10 FPKM mapped to the respective mRNA gene.

iCLIP—iCLIP experiments were performed independently with two different approaches, (*i*) using Ded1p-HTBH and (*ii*) Ded1p-His_6FLAG_3, both on the endogenous *DED1* allele. For iCLIP withDed1p-HTBH, cell growth, crosslinking, and tandem affinity purification on Ni^{2+}-Agarose and Streptavidin beads was performed as described above for the xl-RAP-Seq procedure. Streptavidin beads were washed twice in 1xPNK buffer and split into two samples (80% -"L", 20% -"H"). 200 ng RNAse I was added per gram dry pellet weight to the "L"-sample and 0.1 ng RNAse I to the "H"- sample. The samples were incubated for 5 min at 37°C on a rotator. Resins were subsequently washed with ~1.5 ml wash buffer 2 (2% (w/v) SDS), followed by 1.5 ml wash buffer 2 without SDS, and a wash with1.5 ml 1 x PNK buffer. The supernatant was removed and beads were re-suspended in 67 μl RNase-free water, 3 μl alkaline phosphatase (NEB) and 2 μl RNasin (Roche), and incubated for 20 min at 37°C. Beads were washed twice with 1.5 ml 1 x PNK buffer.

3′-ligation was performed by re-suspending the resin in 32 μl RNase-free water with 8 μl of 20 μM RL3 RNA Linker (Supplementary Information Table S3). Reactions were performed overnight at 4°C in 40 μl, containing 22 μl RNase-free water, 8 μl 10 x T4 RNA ligase buffer, 8 μl BSA (0.2 μg/μl), 3 μl T4 RNA ligase (all NEB).

The resin was washed with 1.5 ml 1 x TEV-salt buffer (50 mM Tris pH 7.5, 300 mM NaCl, 0.5 mM EDTA, 1mM DTT) and twice with 1.5 ml 1 x PNK buffer. Beads were re-suspended in 64 μl RNase-free water, 8 μl 10 x PNK Buffer, 4 μl ^{32}P-γ-ATP, 4 μl T4 PNK (all NEB). Reactions were performed for 50 min in a shaking thermoblock at 37°C. Beads were washed twice with 1.5 ml TEV-salt buffer and twice with 1.5 mlTEV-elution buffer. Beads were subsequently mixed with SDS loading dye and subjected to PAGE on a 10% NEXT gel (Amresco) according to the manufacturer's conditions. Gels were subsequently blotted with nitrocellulose membranes (Amersham™ Protran™, GE Healthcare) and exposed to X-ray film. RNA was then liberated by Proteinase K treatment as described.[37]The purified RNAs were re-suspended in 89 μl RNase- free water, 11 μl 10 x DNase I Buffer, 5 μl RNasin, 5 μl RQ1 DNase (all Promega) and incubated for 20 min at 37°C. The reaction was stopped by standard phenol-chloroform extraction and RNA was ethanol-precipitated overnight.

Author Manuscript Author Manuscript Author Manuscript Author Manuscript

The DNase-treated RNA was re-suspended in 1.4 μl RNase-free water, 0.2 μl 10 mMdNTPs, 1μl 20 nM RT primer X97 (Supplementary Information Table S2), and incubated for 5 min at 65°C. Next, 0.8 μl 5 x first strand buffer, 0.2 μl 1M DTT, 0.2 μl RNase Inhibitor, 0.2 μl Superscript III (all Invitrogen) were added and incubated for 30 min at 50°C. RNA was degraded by alkaline hydrolysis (after addition of 0.5 μl of 1N NaOH and incubation at 98°C for 15 min). After addition of loading buffer, cDNA as applied to 10% denaturing PAGE and staining with SYBR Gold. Fragments of 100 – 125 nt were cut from the gel. The gel slices were crushed and cDNA was recovered by incubation in 500 μl diffusion buffer (20 mM Tris-HCl pH 7.5, 250 mMNaOAc, 1mM EDTA, 0.25% (w/v) SDS) overnight at 4°C, followed by ethanol precipitation.

The cDNA was suspended in 15 μl RNase-free water and circularized with CircLigase I (Epicentre) according to the manufacturer's instructions. The circularized cDNA was utilized for amplification with Phusion polymerase (NEB) and primers X98 and X99 (Supplementary Information Table S2). PCR settings were: 30 s at 98°C, followed by 24 PCR cycles (10 s at 98°C, 30 s at 58°C, 30 s at 72°C). PCR products were applied to 10% non-denaturing PAGE and visualized by SYBR Gold. Products with 75 – 90bp were extracted from cut gel slices, and ethanolprecipitated as described above. PCR products were amplified with Phusion polymerase and primers X100 and X101 for 5 cycles utilizing the same PCR settings as above. PCR products were then separated on a 2% Agarose gel, cut out and subjected to Illumina sequencing using primer X102.

For iCLIP with Ded1p-His_6FLAG_3, cells were grown in SD–TRP media to OD_{600} = 0.5 – 0.6. The culture was subsequently transferred to a 245 mm × 245 mm × 25 mm square Petridish. UV-crosslinking was performed in a Stratalinker 2400 (150 mJ/cm^2, 254nm) at room temperature. Cells were harvested by centrifugation for 5 min at 2000g, washed twice in ice-cold PBS, frozen in liquid nitrogen, and stored at −80°C.

Frozen cells were lysed in CLIP Lysis Buffer (50 mM Tris-HCl, pH 7.8, 300 mM NaCl, 1% Triton X-100, 1 mM PMSF, protease inhibitor cocktail [Roche]) with glass beads six times for 1 min in a Disruptor Genie system (Scientific Industries). Lysates were centrifuged after removal of the glass beads at 10,000 g, twice for 5 min. Cleared lysates (~26.5 A_{260} units) were incubated with anti-FLAG M2 Magnetic Beads (20 μl slurry pre-equilibrated in CLIP Lysis Buffer; Sigma) in a total volume of 1 ml overnight at 4°C. Beads were washed twice in 1 ml FLAG Wash Buffer (50 mM Tris-HCl pH 7.8, 1 M NaCl, 0.1% NP-40) and twice in 1 ml FLAG Elution Buffer (50 mM Tris-HCl pH7.8, 150 mM NaCl, 0.1% NP-40). Proteins were eluted twice in 95 μl FLAG Elution Buffer containing 150 ng/μl 3 x FLAG tag peptide (Sigma). Pooled eluates were incubated with 10μl RNase I (Ambion), diluted 1:500,000 in FLAG Elution Buffer for 15 min at room temperature. Reactions were quenched with 960 μl 8 M guanidine-HCl, 90 μl Dilution Buffer (600 mM Tris-HCl pH 7.8, 3.93 M NaCl), 6.4 μl 2 M imidazole, 10.8 μl 10% NP-40 and 12.8 μl 500 mM beta-mercaptoethanol. RNase-treated eluates were incubated further with Ni- NTA Magnetic Agarose Beads (50 μl slurry pre-equilibrated in Ni-NTA Binding Buffer [50mM Tris-HCl pH 7.8, 300mM NaCl, 10mM imidazole, 6 M guanidine-HCl, 0.1% NP-40, 5mM beta- mercaptoethanol]; Qiagen) overnight at 4°C.

Author Manuscript Author Manuscript Author Manuscript Author Manuscript

Ni^{2+}-beads were washed twice in 1 ml CLIP Wash Buffer I (50mM Tris-HCl pH 7.8, 500mM NaCl, 10mM imidazole, 6M guanidine-HCl, 0.1% NP-40, 5mM beta-mercaptoethanol) and three times in 1ml 1 x PNK Buffer (50 mM Tris-HCl pH 7.8, 10 mM $MgCl_2$, 0.5% NP-40, 10 mM beta- mercaptoethanol). Beads were subsequently incubated with 30 µl Dephosphorylation Mix (50 mMTris-HCl pH 7.8, 10 mM $MgCl_2$, 10 mM beta-mercaptoethanol, 3 M BU TSAP [Promega], 30U SUPERase-In [Ambion]) for 30 min at 37°C in a Thermomixer at 1000 rpm. Reactions were terminated by adding 1 ml CLIP Wash Buffer I, and beads were washed three times in 1 ml 1 x PNK Buffer, re-suspended in 30 µl Ligation Mix (50 mM Tris-HCl, pH 7.8, 10 mM $MgCl_2$, 10 mM beta-mercaptoethanol, 10% PEG8000 [NEB], 10% DMSO, 2 µM 3′ adenylated adapter X103, 30U T4 RNA Ligase 1 [NEB], 30 U SUPERase-In [Ambion]) and incubated for 3 h at 22°C in a thermomixer at 1000 rpm. Reactions were terminated by adding 1ml CLIP Wash Buffer I. Beads were washed three times in 1ml 1 x PNK Buffer, re-suspended in 30 µl Kinase Mix (50 mM Tris-HCl, pH 7.8, 10 mM $MgCl_2$, 10 mM beta-mercaptoethanol, 30 U PNK [NEB], 5 µCi γ-^{32}P-ATP, 30 U SUPERase-In [Ambion]) and incubated for 30 min at 37°C in a thermomixer (1000 rpm). Reactions were terminated adding 1 ml CLIP Wash Buffer I. Beads were washed three times in 1mL CLIP Wash Buffer I, and three times in 1 ml CLIP Wash Buffer II (50 mM Tris-HCl, pH 7.8, 50 mM NaCl, 10 mM imidazole, 0.1% NP-40, 5 mM beta-mercaptoethanol). Proteins were eluted with 35 µl CLIP Wash Buffer II containing 200 mM imidazole 3 times for 5 min at 22°C in a thermomixer (1000 rpm).

Pooled eluates were digested with Proteinase K (Invitrogen) at 50°C for 1h. The reaction was stopped by standard phenol/chloroform extraction. Released RNA was precipitated by ethanol precipitation overnight in the presence of 1µl GlycoBlue (Ambion) and 1pmol reverse- transcription DNA primer X104. RNA was converted to first-strand cDNA in a 10 µl standard reaction mix with 0.5 µl Superscript III (Invitrogen) and the co-precipitated DNA primer. The reaction conditions were as follows: 25°C for 5 min, 42°C for 20 min, 50°C for 40 min. RNA degraded with 1.67 µl of 1 M NaOH for 10 min at 90°C. The cDNA was ethanol precipitated with GlycoBlue for >2h. cDNA fragments of 120–200 nt were gel purified on a urea-denaturing 6% acrylamide gel and ethanol precipitated with GlycoBlue overnight. cDNA was circularized in a 10 µl reaction mix using 0.5 µlCircLigase I (Epicentre) in the presence of 1 M betaine at 60°C for 1hr. The reaction was then supplemented with additional 0.5 µl CircLigase I and incubated at 60°C for 1hr. The enzyme was inactivated at 80°C for 10 min. PCR and formamide-gel purification of PCR products were performed as described [38], using 20 cycles of PCR and isolating 120–200 nucleotide ssDNA fragments.

Sequencing reads were processed as described previously [37,39]. Briefly, after trimming of adaptor sequences, reads were mapped to sacCer3 with Bowtie2 or TopHat software with similar settings used for Ribosome profiling data, outlined above. Identical reads were subsequently collapsed and duplications removed. The crosslink position of Ded1p to RNA was defined as 1 nt 5′ of the 5′ mapped nucleotide of a sequencing read.[37]

DMS-MaPseq—Yeast strains (WT-DED1 and *ded1-95*) were grown in YPD at 30°C. Overnight cultures were diluted to OD_{600} of ~ 0.09 and grown to an OD_{600} = 0.6. An equal volume of 44°C YPD media was added to achieve an immediate temperature shift to 37°C,

Author Manuscript Author Manuscript Author Manuscript Author Manuscript

as outlined for the ribosome profiling experiments. Cultures were incubated in a 37°C water bath for 3 min. At this time, dimethyl sulfate (DMS, Sigma) was added to a 5% (v/v) final concentration and incubation was continued with stirring for 3 min. DMS was quenched by adding 30 ml of ice-cold stop solution (30% β-mercaptoethanol, 50% (v/v) isoamyl alcohol). Cells were quickly transferred to ice, collected by centrifugation at 3,500 g at 4°C for 4 min, and washed with 10 ml 30% β-mercaptoethanol solution. Cells were re-suspended in 0.6 ml RNA lysis buffer (6 mM EDTA, 45 mMNaOAc, pH 5.5). Total RNA was purified with hot acid phenol (Ambion) and ethanol precipitation. Sequencing libraries were prepared as previously described.[17]

Raw fastq files were stripped of linker sequences and filtered for overall quality using the FASTX-Toolkit Clipper and Quality Filter functions (http://hannonlab.cshl.edu/fastx_toolkit/), respectively, requiring that 80% of sequenced bases have a quality score >25. Reads were aligned against the yeast genome (sacCer3) using Tophat v2.1.0 with bowtie2 with the following settings for a 50 bp sequencing run: --no-novel-juncs -N 5 --read-gap-length 7 --read-edit-dist 7 --max-insertion-length 5 --max-deletion-length 5 -g 3. All non-uniquely aligned reads were then removed. Due to empirically determined mutation enrichment from non-template addition, we trimmed 2 nucleotides from the 5′ end of each read. Mismatches located within 3 nucleotides of an indel were also discarded for future analysis.

Bioinformatic analyses—Yeast genomic sequence conservation scores were obtained from *Saccharomyces cerevisiae* genome database (www.yeastgenome.org). Positional coordinates of mRNAs including transcription start sites and polyadenylation sites are based on sacCer3 and reported measurement.[40] Genome-wide datasets were visualized by IGV software [41]. Structural models of the small and large ribosomal subunits including initiation factors were generated with the Chimera software.[30,42] Analyses of Gene Ontology term enrichment were carried out with GOrilla software utilizing a single ranked list of genes.[43]

RNA structure prediction was carried out with sequences 0 – 99 nt 3′ of the first nucleotide of an alternative start codon using the RNAfold web server.[44] Constraint settings were derived from DMS-MaPseq data as follows: a nucleotide was set as “unpaired” if the DMS-MaPseq counts of a given nucleotide exceeded the value of 0.49 relative to the third highest count number in the range of 100 nt downstream of an aTIS.

Statistical significance of enrichment or depletion in certain regions (e.g. Figs. 2c, 3d,e, Extended data Fig. 10a) was determined by comparing weighted data vectors of the observed variable to the background value. To this end, we calculated t-values with the *wtd.t.test* – function in R. The algorithm is based on the mean and 1/(standard errors)^2 as estimate of the means accuracy. The given p-values correspond to a two-tailed t-test.

Further bioinformatic analyses and multiple linear regressions were performed with R with customized scripts using RStudio Software.[45,46] Code is available upon request. Normalization of datasets including ribosome protected fragments, monosome-protected fragments, Ded1p iCLIP-Seq and DMS-MaPseq counts were performed relative to the total number of counts of the entire mRNA.[42]

Author Manuscript Author Manuscript Author Manuscript Author Manuscript

To compute Ded1p binding density, DMS-MapSeq ratios, or sequence conservation values in the vicinity of aTIS, it was important to normalize for inherent positional trends within the exact region in the respective iCLIP, DMS-MapSeq and sequence conservation datasets. For example, values for DMS-MapSeq ratios (counts $^{ded1\text{-}95}$/counts ^{WT}), and iCLIP reads show an upward trend with increasing distance from the 5′ cap in 5′UTRs. To normalize for inherent positional trends, we calculated a background distribution for the vicinity of each aTIS. We randomly choose a position in the respective section of a given mRNA, and determined the signal distribution in the vicinity of this position (for example, position -5 relative to the 5′ nt of an aTIS). This process was repeated four times. The background value reflects the average of these five calculated values. Reported enrichment values represent the ratio of the measured signal over the background value at each indicated position. Values are given in all plots as $\log_2$ (signal^{measured}/signal^{background}). Statistical significance of enrichment or depletion was determined by calculating the t-value of the observed variable based on the mean and standard deviation ofthe background value.

Metagene profiles were calculated by averaging normalized Ded1p iCLIP counts and DMS-MaPseq counts after binning transcript coordinates from 5′UTRs, ORFs and 3′UTRs in bins reflecting 2% of each section of mRNA. Ded1p binding sites and the midpoint of RNA secondary structures were determined by Piranha peak calling software (http://smithlabresearch.org).

Calling parameters were optimized based on visual inspection. To call peak sites of RNA secondary structures, a genome-wide dataset of $\log_2$(counts of DMS-MaPseq $^{WT/ded1\text{-}95}$) was utilized as input file.

Data Availability

The data that support the findings of this study have been deposited in the Gene Expression Omnibus (GEO) repository with the accession code GSE93959. All other data are available from the corresponding author upon reasonable request.

Author Manuscript Author Manuscript Author Manuscript Author Manuscript

Extended Data

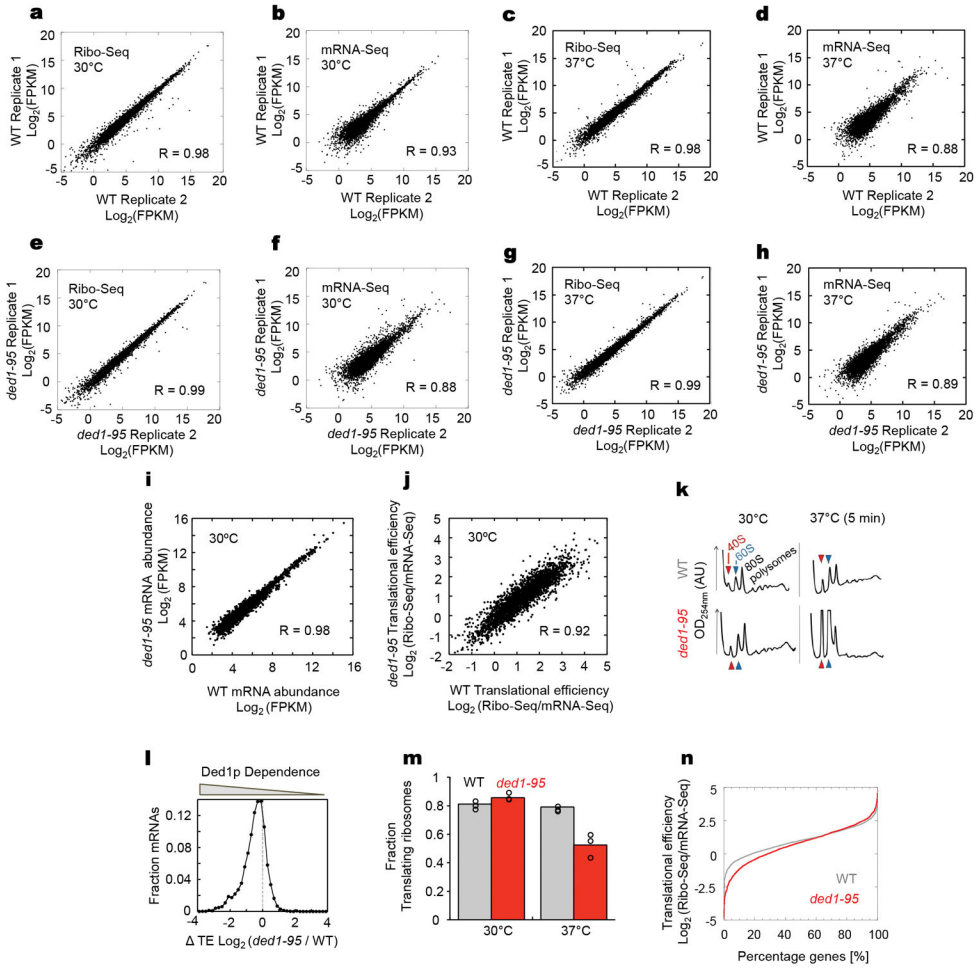

Extended Data Figure 1. mRNA expression, and translation profiles in WT *DED1* and *ded1-95*

a, Correlation of ribosome footprint counts between two biological replicates in WT *DED1* at 30°C (N = 5,523; R: Pearson correlation coefficient).

b, Correlation of mRNA expression levels between two biological replicates in WT *DED1* at 30°C (N = 5,372)

c, Correlation of ribosome footprint counts between two biological replicates in WT *DED1*, 5 min after temperature shift to 37°C (N = 5,523).

d, Correlation of mRNA expression levels between two biological replicates in WT *DED1*, 5 min after temperature shift to 37°C (N = 5,372)

e, Correlation of ribosome footprint counts between two biological replicates in *ded1-95* at 30°C (N = 5,523)

f, Correlation of mRNA expression levels between two biological replicates in *ded1-95* at 30°C (N = 5,372)

g, Correlation of ribosome footprint counts between two biological replicates in *ded1-95*, 5 min after temperature shift to 37°C (N = 5,523)

Author Manuscript Author Manuscript Author Manuscript Author Manuscript

h, Correlation of mRNA expression levels between two biological replicates in *ded1-95*, 5 min after temperature shift to 37°C (N = 5,372)
i, Correlation of mRNA expression levels between WT *DED1* and *ded1-95* at 30°C (N = 2,976). Each datapoint represents the average of at least two replicates.
j, Correlation of translational efficiencies between WT *DED1* and *ded1-95* at 30°C (N = 2,976). Each datapoint represents the average of at least two replicates.
k, Representative polysome profiles of WT *DED1* and *ded1-95* strains at 30°C and 5 min after shift to 37°C. Similar results were obtained in three independent experiments.
l, Changes in translational efficiencies (ΔTE) for mRNAs in *ded1-95*, compared to WT *DED1*, 5 min after temperature shift (mean of two biological replicates). The dotted line indicates no change.
m, Fraction of 18S rRNA in polysome fractions, compared to the entire sample, at 30°C and 5 minutes after temperature shift to 37°C. Each bar represents the average of three independent experiments. Empty circles represent each replicate.
n, Cumulative distribution of translational efficiencies of WT *DED1* and *ded1-95*, 5 minutes after temperature shift to 37°C (N = 2,976). Each datapoint represents the average of at least two replicates.

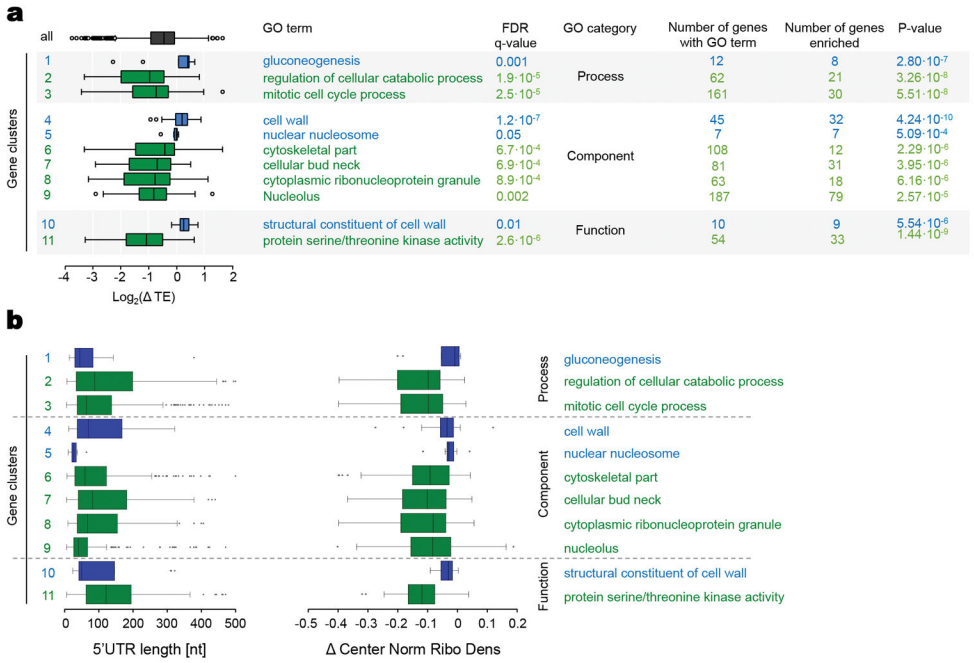

Extended Data, Figure 2. A subset of mRNAs is largely insensitive to Ded1p
a, GO term defined mRNA groups whose translation are strongly impacted (green) or largely unaffected by Ded1p (blue). Boxplots (group median) of changes in translational efficiencies (ΔTE, box boundaries: upper and lower quartiles, error bars: 1.5 x interquartile range). The black boxplot marks changes in translational efficiencies for all mRNAs (Fig. 1b). mRNAs for each GO-term were extracted from the SGD[47]. The FDR q-value indicates the enrichment p-value according to a hypergeometric model after correction for multiple testing using the Benjamini and Hochberg method[48].

b, Boxplots (as in panel **a**) of 5′UTR lengths and median of the shift in the normalized center of ribosome density (Fig. 1b) for GO term defined mRNA groups, color-coded as in panel (**a**).

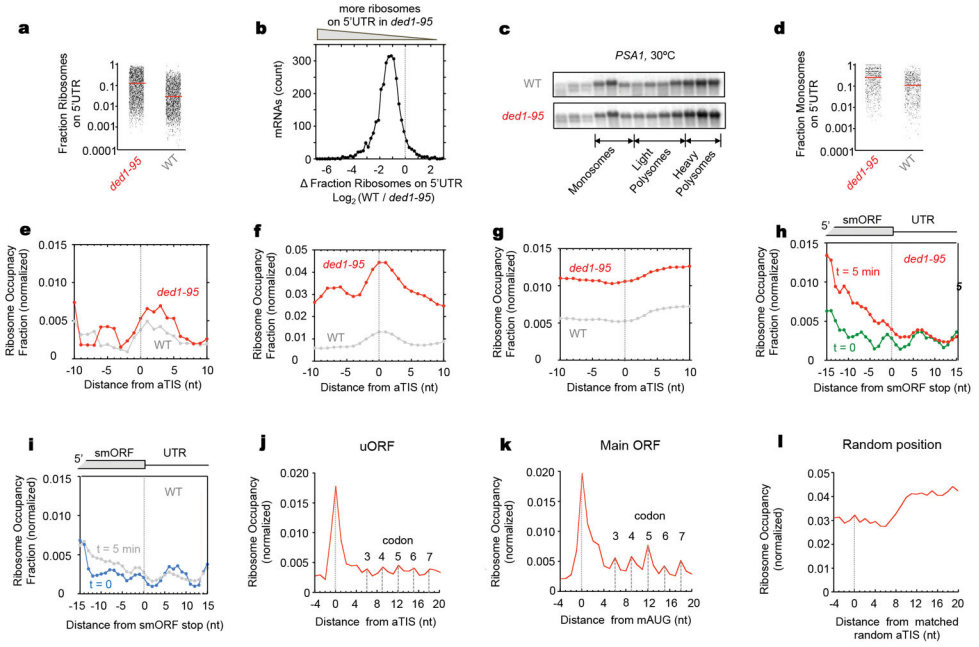

Extended Data, Figure 3. Activation of aTIS in *ded1-95* upon temperature shift

a, Fraction of ribosome footprints on 5′UTRs in WT *DED1* and *ded1-95*, (5 min, 37°C, N = 3,273). The red line indicates the mean. Statistical significance for the difference between *ded1-95* and WT *DED1*: p = 1.2e-119 (two tailed t-test). A similar result was obtained in an independent replicate (p = 5.4e-47).

b, Changes in the fraction of ribosomes on 5′UTRs for all mRNAs (N = 2,660) in WT *DED1* compared to *ded1-95*, 5 min after temperature shift to 37°C. The values on the x-axis represent the ratio ($\log_2$) of the fraction of ribosomes on each 5′UTR in WT, divided by the fraction of ribosomes on the same 5′UTR in *ded1-95*. Each value represents the average of two independent biological replicates.

c, Representative Northern blots of PSA1 after sucrose gradient centrifugation for WT *DED1* and *ded1-95*, at 30ºC. A similar result was obtained in an independent biological replicate.

d, Fraction of ribosome footprints on 5′UTRs in WT *DED1* and *ded1-95*, (5 min, 37°C), measured only in 80S monosomes (N = 973, reads from two independent experiments combined). Statistical significance for the difference between *ded1-95* and WT *DED1*: p = 1.2e-50 (two tailed t-test).

e, Mean ribosome occupancy within 10 nt 3′ and 5′ of the high confidence aTIS in 5′UTRs (moving average: ± 1nt, 5 min, 37°C), measured without cycloheximide.

f, Mean ribosome occupancy within 10 nt 3′ and 5′ of the high confidence aTIS in 5′UTRs (N = 274) in 80S monosomes (moving average: ± 1nt, 5 min, 37°C).

Author Manuscript Author Manuscript Author Manuscript Author Manuscript

Author Manuscript Author Manuscript Author Manuscript Author Manuscript

g, Mean ribosome occupancy within 10 nt 3′ and 5′ of all near cognate initiation codons (N = 61,614; excluding medium confidence aTIS) in 5′UTRs (moving average: ± 1nt, 5 min, 37°C).

h, Ribosome occupancy of 3′ ends in small upstream open reading frames (smORFs) initiating at high confidence aTIS in *ded1-95* before (t = 0) and after (t = 5 min) temperature shift. SmORFs were included in this analysis if its length exceeds 3 codons and if the smORF terminates at least 11 nt upstream of the main AUG (N = 76).

i, Ribosome occupancy of 3′ ends of smORFsdefined in panel (**e**) in WT *DED1* before (t = 0) and after (t = 5 min) temperature shift.

j, Ribosome occupancy 4 nt 5′ and 20 nt 3′ of high confidence aTIS on 5′UTRs (N = 274) for *ded1-95*, 5 min after temperature shift. The dashed lines indicate the first nucleotide of the marked in-frame codons.

k, Ribosome occupancy 4 nt 5′ and 20 nt 3′ of the main AUG of mRNAs containing high confidence aTIS on 5′UTRs for *ded1-95*, 5 min after temperature shift. For mRNAs with multiple high confidence aTIS in their 5′UTR, the main AUG was counted only once. The dashed lines indicate the first nucleotide of the marked in-frame codons.

l, Ribosome occupancy 4 nt 5′ and 20 nt 3′ of high confidence aTIS-matched random position (averaged from five randomizations) on 5′UTRs (N = 274) for *ded1-95*, 5 min after temperature shift. The dashed line indicates the first nucleotide.

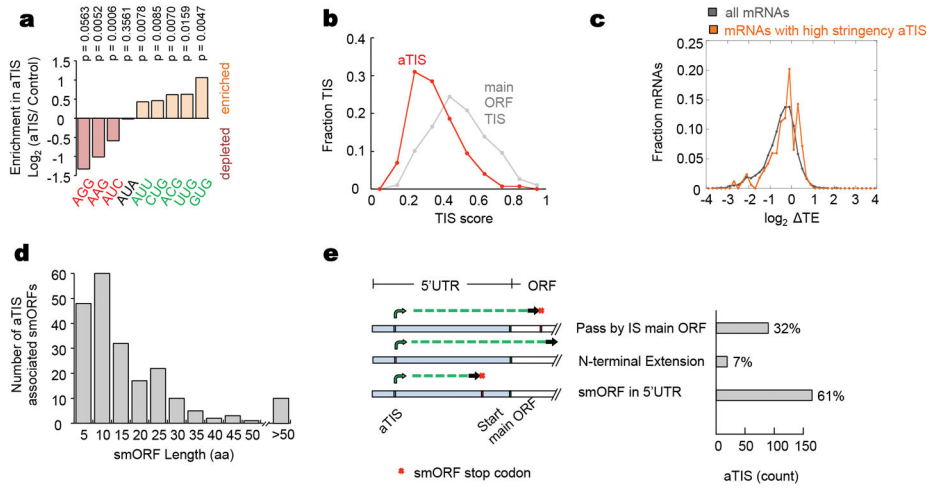

Extended Data, Figure 4. Characteristics of small open reading frames associated with activated aTIS

a, Enrichment or depletion of each near-cognate codon in aTISs over the background distribu- tion of the codon (p values determined according to a two-tailed t-test).

b, Mean translation initiation site score (positions −6 to +6, excluding +1 to +3) calculated according to Miyasaka[49] for high stringency aTIS (N = 274, red), and TIS of main ORFs (N = 4,972, grey). A TIS score exceeding 0.01 is considered a potential translational initiation site[14].

c, Changes in translational efficiencies (ΔTE) for mRNAs in *ded1-95*, compared to WT DED1, 5 min after temperature shift for all mRNAs (Fig. 1b) and aTIS-containing mRNAs.

Author Manuscript Author Manuscript Author Manuscript Author Manuscript

d, Length of the small open reading frames (smORFs) associated with *ded1-95*-activated aTIS. SmORFs encoding N-terminal extensions were excluded from the analysis.
e, Type of smORFs associated with *ded1-95*-activated aTIS. The bargraphs show the fraction of smORFs that falls into each category. The distribution of changes in translation efficiency (ΔTE) for RNAs with either type of smORF did not differ significantly.

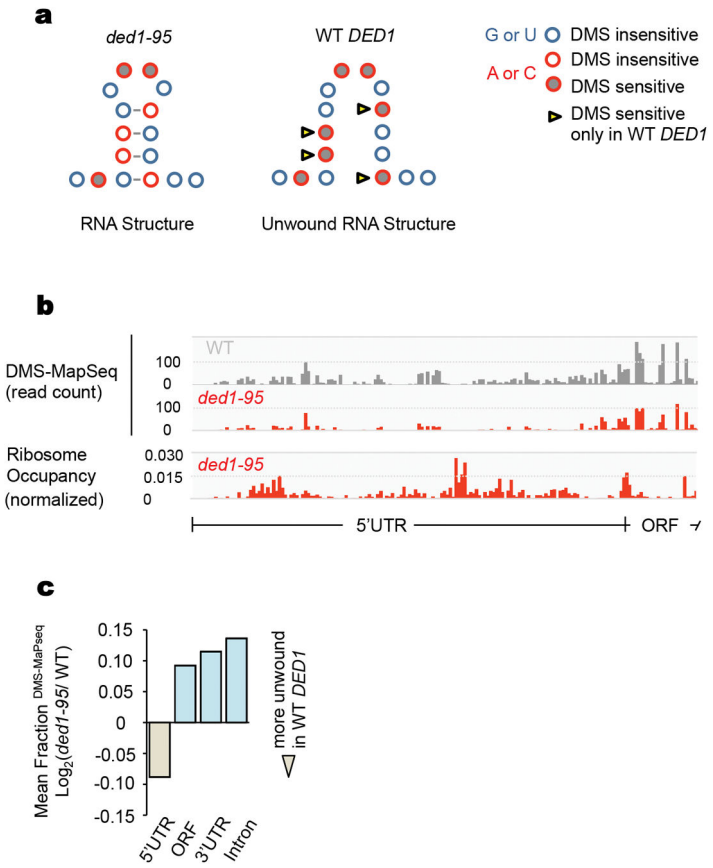

Extended Data, Figure 5. mRNA structure unwinding by Ded1p in cells using DMS MaPSeq
a, Schematic for DMS-MaPseq approach to monitor RNA structure unwinding by Ded1p). All DMS-MapSeq experiments were performed 5 minutes after temperature shift.
b, Representative DMS MaPSeq tracks in the PSA1 5′UTR 5 min after temperature shift for WT *DED1* (grey) and *ded1-95* (red). Bars show normalized RT stops. A similar result was obtained in an independent replicate. The Average Pearson correlation coefficient of DMS-MaPseq counts per 5′UTR between two replicates (5 min after temperature shift to 37°C) is for WT: R = 0.57 (N = 864), and for *ded1-95*: R = 0.63 (N = 692). The ribosome occupancy track for *ded1-95* is shown for reference.
c, Unwinding of mRNA structure by Ded1p for different mRNA regions. Similar results were obtained in two independent experiments.

Author Manuscript Author Manuscript Author Manuscript Author Manuscript

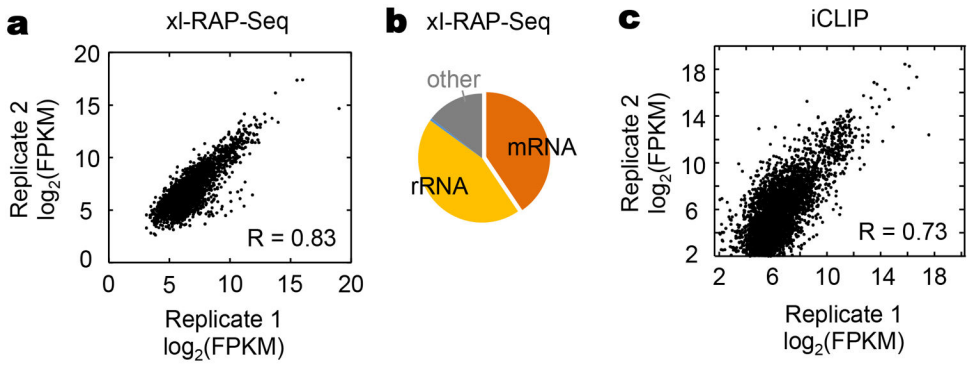

Extended Data, Figure 6. xl-RAP-Seq and iCLIP

a, Correlation of sequence reads (FPKM) per mRNA for two independent biological xl-RAP-Seq replicates (N = 2,992, R: Pearson Correlation Coefficient)

b, Fraction of mRNA (40%) and rRNA (44%) crosslinked to WT Ded1p as fraction of all sequencing reads (mean of two independent experiments). N = 4,280 mRNAs exceed a minimal read count of FPKM ≥ 10.

c, Correlation of the number of RT stops (FPKM) per mRNA for the two independent iCLIP approaches (Replicate 1:Flag-tagged Ded1p, Replicate 2: HTBH-tagged Ded1p, N = 4,007, R: Pearson Correlation Coefficient)

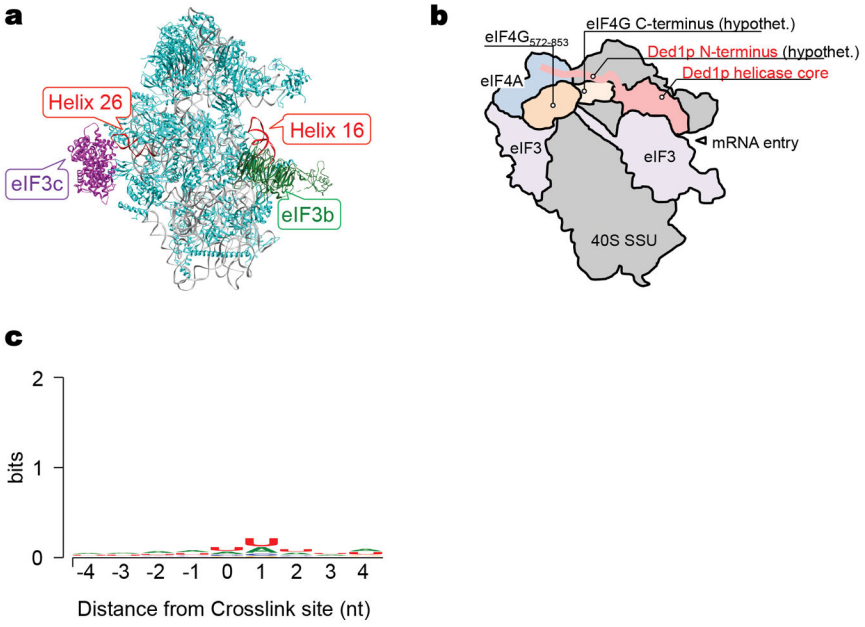

Extended Data, Figure 7. Ded1p binding sites on 18S RNA and mRNAs

a, Ded1p binding sites on Helix 720 (exit) and Helix 16 (entry) (red) are in close proximity to binding sites of eIF3c (purple) and eIF3b (green) on the 40S ribosomal subunit (rRNA: grey, ribosomal proteins: cyan)[42].

b, Localization of Ded1p (apricot) on Helix 16 of the PIC. (Schematic model of the yeast PIC with eIF3: http://www.bangroup.ethz.ch/research/eukaryotic_translation_initiation.html and references therein, position of eIF4G$^{572-853}$ and eIF4A (Ref.[50]). The position of the

Author Manuscript Author Manuscript Author Manuscript Author Manuscript

eIF4G C- terminus is hypothetical. The helicase core of Ded1p was modeled in analogy to the DDX3 core structure[51], with the RNA binding site in contact with Helix16 at the main iCLIP crosslink sites. The position of the low complexity N-terminus of Ded1p is hypothetical.

c, Sequence logo of Ded1p binding sites on mRNAs.Sets of 10^4 binding sites were randomly sampled from all Ded1p crosslinking sites and used as input to create a sequence logo (http://weblogo.berkeley.edu). All subsets yielded essentially the same sequence logo as shown here. Position zero denotes the RT stop.

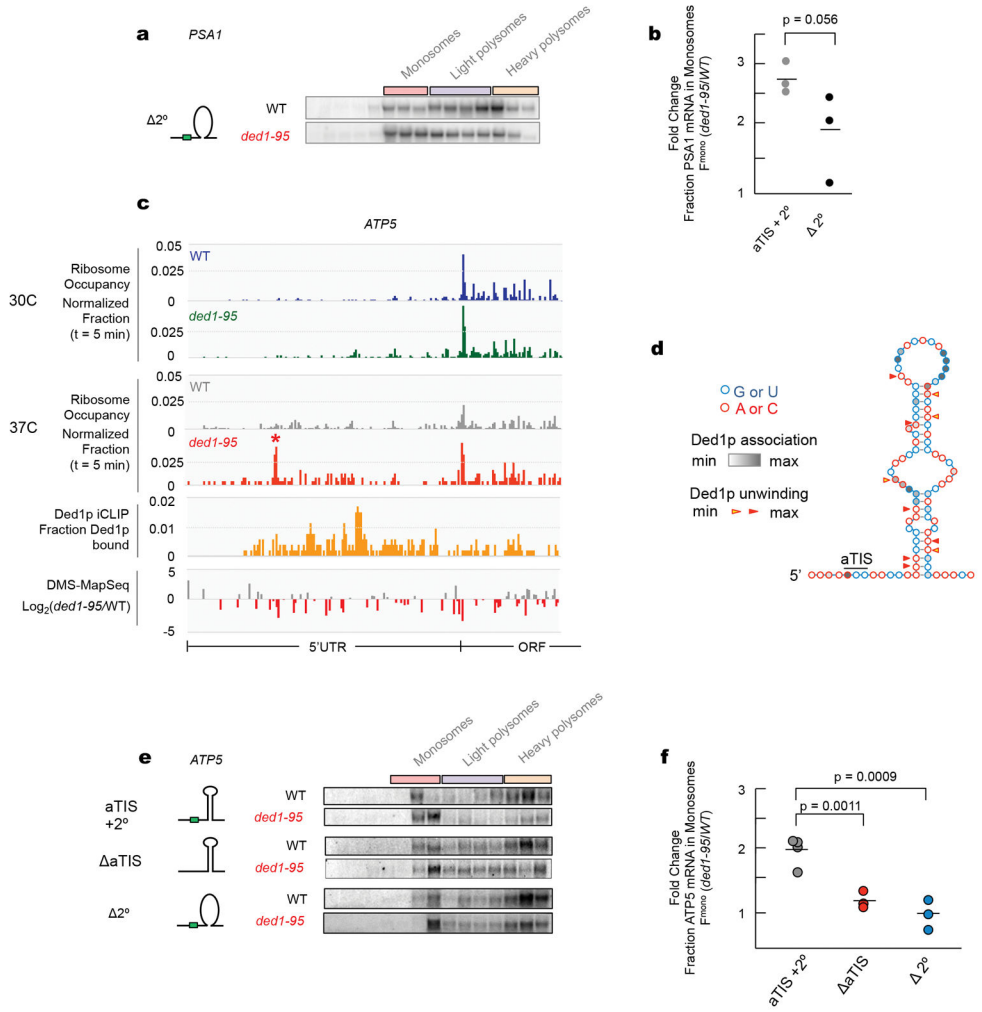

Extended Data, Figure 8. Representative Northern Blots of PSA1 (Δ2º) and ATP5 (ΔaTIS, Δ2º) for WT *DED1* and *ded1-95*

a, Representative RNA blots (5 min, 37ºC) for the PSA1 mRNA with altered secondary structure, 3′ of the aTIS (Δ2º). Similar results were obtained in three independent biological replicates.

b, Quantification of RNA blots for accumulation of the PSA1 Δ2º mRNA in Monosomes in *ded1-95*, compared to WT *DED1*. The line indicates the average. The p-value for the difference in monosome accumulation was determined by a one-tailed t-test.

Author Manuscript Author Manuscript Author Manuscript Author Manuscript

c, Representative ribosome profiling tracks for the 5′UTR of ATP5 in WT *DED1* and *ded1-95* (30°C and after temperature shift). The near-cognate initiation codon is highlighted by a star. For comparison, Ded1p crosslinking (yellow track) and differential DMS-MaPseq tracks ([$\log_2$(*ded1-95*/WT)], unwound mRNA regions marked by red bars, negative values) for the 5′UTR of the ATP5 mRNA are shown. Similar results were obtained in two independent experiments.

d, DMS-MapSeq constrained secondary structure model of a fragment of the ATP5 mRNA 5′UTR. The aTIS is marked by a line. Ded1p crosslinking (iCLIP) and unwinding (DMS-MapSeq) for each nucleotide are indicated. The ratio of normalized DMS-MapSeq counts of WT/*ded1-95* in two categories: yellow triangles: 0.6 – 1.0 (moderately unwound), and red triangles: > 1.0 (strongly unwound).

e, Representative RNA blots (5 min, 37ºC) for ATP5 mRNA WT, with mutations in the aTIS (ΔaTIS) and with altered secondary structure, 3′ of the aTIS (Δ2º) for WT *DED1* and *ded1-95*. Similar results were obtained in three independent experiments.

f, Quantification of RNA blots for accumulation of the ATP5 ΔaTIS and Δ2º mRNA in Monosomes in *ded1-95*, compared to WT *DED1*. The lines indicate the averages. p-values were determined by a one-tailed t-test.

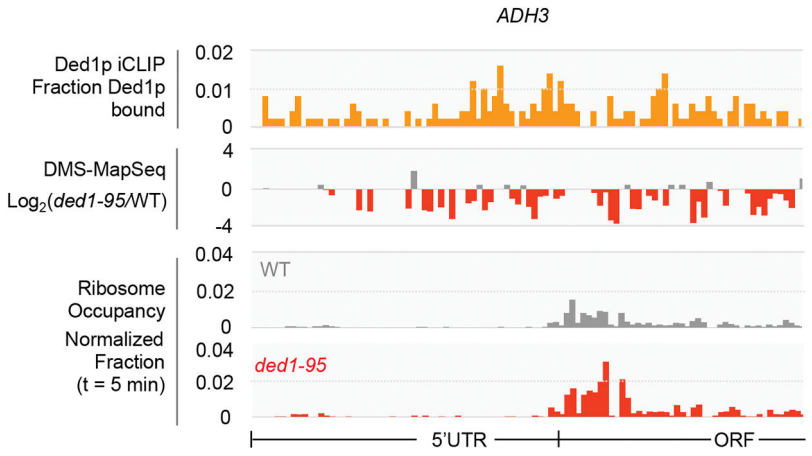

Extended Data, Figure 9. Ded1p binding and mRNA remodeling can occur without decreased translation efficiency if nonear-cognate initiation codon is present

Ded1p iCLIP track, differential DMS-MaPseq track (5 min, 37ºC) and ribosome occupancy tracks (5 min, 37ºC) of WT *DED1* and *ded1-95* for ADH3 mRNA, whose translation is largely unaffected by Ded1p (ΔTE = − 0.1). 5′UTR and ORF are marked. iCLIP and DMS-MaPseq tracks show Ded1p binding and remodeling of the 5′UTR, ribosome profiling tracks indicate no significant accumulation of ribosomes in the 5′UTR. Similar results were obtained in two independent experiments.

Author Manuscript Author Manuscript Author Manuscript Author Manuscript

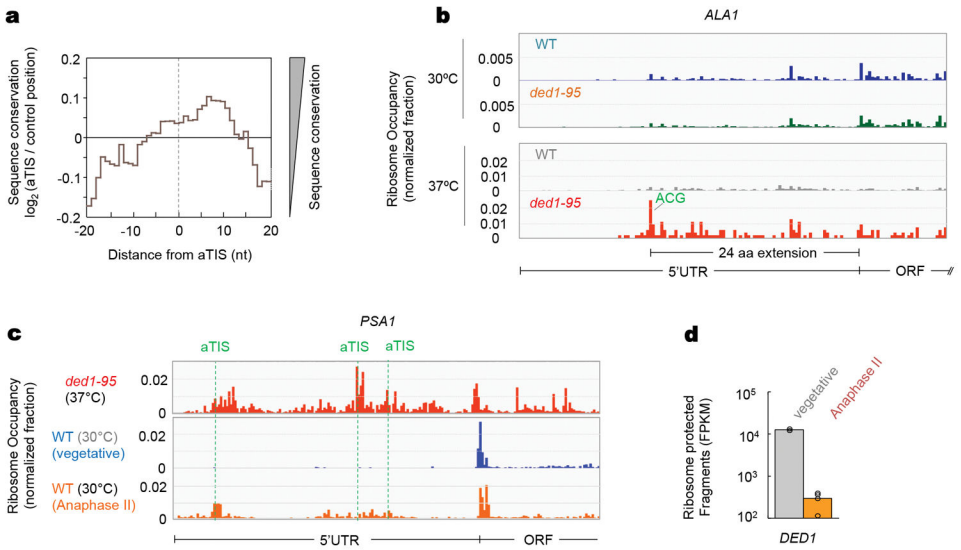

Extended Data, Figure 10. aTIS conservation across fungi and Ded1p-mediated activation of uORFs starting from near-cognate initiation codons

a, Sequence conservation in *fungi* around high confidence aTIS (moving average of ± 1 nt). Positive values indicate higher sequence conservation than the average of five randomly chosen positions on the same 5′UTR for each aTIS, negative values indicate less sequence conservation (conservation scores were obtained from the sacCer3 phastCons7way dataset, based on sequence homology between following species: *S. cerevisiae, S. paradoxus, S. katae, S. kudriavzevii, S. bayanus, S. castelli, S. kluyveri*)[52].

b, Ribosome occupancy tracks (30ºC and 5 min, 37ºC) of WT *DED1* and *ded1-95* for ALA1 mRNA. 5′UTR and ORF are marked. The ACG initiation codon (−25, highlighted by star) has been previously shown to function as aTIS for the mitochondrial isoform of Ala1p (Ref. [29]). Similar results were obtained in two independent biological replicates for each experiment.

c, Ribosome occupancy tracks (5 min, 37ºC) of *ded1-95* and WT *DED1* (vegetative control and Anaphase II) for *PSA1* mRNA. aTISs are marked by dashed lines. Similar results were obtained in two (vegetative control) and four (Anaphase II) independent experiments.

d, Ribosome-protected fragments mapping to *DED1* in vegetative cells and cells in Anaphase II (average of two [vegetative] and four [Anaphase II] independent experiments, circles represent each replicate).

Supplementary Material

Refer to Web version on PubMed Central for supplementary material.

Acknowledgments

This study was supported by the NIH (GM118088 to E.J., GM107331 to D.D.L.) and by a postdoctoral fellowship from the German Research Council (GU 1146/1-1 to U.P.G.). D.P.B. and J.S.W. are investigators of the HHMI. We thank Mark Adams for help with initial data analysis; Najwa Al-Huseini and Jeff Coller for discussion and materials; AkshayTambe, Molly Hannigan, and Rolf Backofen for advice on bioinformatic data analysis, Bernd Klaus for critical advice on statistical analysis and Matthias Hentze for discussion.

Author Manuscript Author Manuscript Author Manuscript Author Manuscript

References

1. Sharma D, Jankowsky E. The Ded1/DDX3 subfamily of DEAD-box RNA helicases. Crit Rev Biochem Mol Biol. 2014; 49:343–360. DOI: 10.3109/10409238.2014.931339 [PubMed: 25039764]
2. Bol GM, Xie M, Raman V. DDX3, a potential target for cancer treatment. Mol Cancer. 2015; 14:188. [pii]. [PubMed: 26541825]
3. Oh S, et al. Medulloblastoma-associated DDX3 variant selectively alters the translational response to stress. Oncotarget. 2016; 7:28169–28182. [pii]. DOI: 10.18632/oncotarget.86128612 [PubMed: 27058758]
4. Pugh TJ, et al. Medulloblastoma exome sequencing uncovers subtype-specific somatic mutations. Nature. 2012; 488:106–110. [pii]. DOI: 10.1038/nature11329nature11329 [PubMed: 22820256]
5. Snijders Blok L, et al. Mutations in DDX3X Are a Common Cause of Unexplained Intellectual Disability with Gender-Specific Effects on Wnt Signaling. Am J Hum Genet. 2015; 97:343–352. [pii]. DOI: 10.1016/j.ajhg.2015.07.004S0002-9297(15)00280- [PubMed: 26235985]
6. Valiente-Echeverria F, Hermoso MA, Soto-Rifo R. RNA helicase DDX3: at the crossroad of viral replication and antiviral immunity. Rev Med Virol. 2015; 25:286–299. DOI: 10.1002/rmv.1845 [PubMed: 26174373]
7. Ingolia NT, Brar GA, Rouskin S, McGeachy AM, Weissman JS. The ribosome profiling strategy for monitoring translation in vivo by deep sequencing of ribosome-protected mRNA fragments. Nat Protoc. 2012; 7:1534–1550. [pii]. DOI: 10.1038/nprot.2012.086nprot.2012.086 [PubMed: 22836135]
8. Putnam AA, et al. Division of Labor in an Oligomer of the DEAD-Box RNA Helicase Ded1p. Mol Cell. 2015; 59:541–552. [pii]. DOI: 10.1016/j.molcel.2015.06.030S1097-2765(15)00524-9 [PubMed: 26212457]
9. Burckin T, et al. Exploring functional relationships between components of the gene expression machinery. Nat Struct Mol Biol. 2005; 12:175–182. nsmb891 [pii]. DOI: 10.1038/nsmb891 [PubMed: 15702072]
10. Chuang RY, Weaver PL, Liu Z, Chang TH. Requirement of the DEAD-Box protein ded1p for messenger RNA translation. Science. 1997; 275:1468–1471. [PubMed: 9045610]
11. Sen ND, Zhou F, Ingolia NT, Hinnebusch AG. Genome-wide analysis of translational efficiency reveals distinct but overlapping functions of yeast DEAD-box RNA helicases Ded1 and eIF4A. Genome Res. 2015; 25:1196–1205. [pii]. DOI: 10.1101/gr.191601.115gr.191601.115 [PubMed: 26122911]
12. Heyer EE, Moore MJ. Redefining the Translational Status of 80S Monosomes. Cell. 2016; 164:757–769. [pii]. DOI: 10.1016/j.cell.2016.01.003S0092-8674(16)00004-0 [PubMed: 26871635]
13. Hinnebusch AG, Ivanov IP, Sonenberg N. Translational control by 5′-untranslated regions of eukaryotic mRNAs. Science. 2016; 352:1413–1416. [pii]. DOI: 10.1126/science.aad9868352/6292/1413 [PubMed: 27313038]
14. Ingolia NT, Ghaemmaghami S, Newman JR, Weissman JS. Genome-wide analysis in vivo of translation with nucleotide resolution using ribosome profiling. Science. 2009; 324:218–223. [pii]. DOI: 10.1126/science.11689781168978 [PubMed: 19213877]
15. Brar GA, et al. High-resolution view of the yeast meiotic program revealed by ribosome profiling. Science. 2012; 335:552–557. DOI: 10.1126/science.1215110 [PubMed: 22194413]
16. Kolitz SE, Takacs JE, Lorsch JR. Kinetic and thermodynamic analysis of the role of start codon/anticodon base pairing during eukaryotic translation initiation. RNA. 2009; 15:138–152. [pii]. DOI: 10.1261/rna.1318509rna.1318509 [PubMed: 19029312]
17. Berthelot K, Muldoon M, Rajkowitsch L, Hughes J, McCarthy JE. Dynamics and processivity of 40S ribosome scanning on mRNA in yeast. Mol Microbiol. 2004; 51:987–1001. [PubMed: 14763975]
18. Zubradt M, et al. DMS-MaPseq for genome-wide or targeted RNA structure probing in vivo. Nature Methods. 2017; 14:75–82. DOI: 10.1038/nmeth.4057 [PubMed: 27819661]

Author Manuscript Author Manuscript Author Manuscript Author Manuscript

19. Huppertz I, et al. iCLIP: protein-RNA interactions at nucleotide resolution. Methods. 2014; 65:274–287. [pii]. DOI: 10.1016/j.ymeth.2013.10.011S1046-2023(13)00414-3 [PubMed: 24184352]
20. Hinnebusch AG. The scanning mechanism of eukaryotic translation initiation. Annu Rev Biochem. 2014; 83:779–812. DOI: 10.1146/annurev-biochem-060713-035802 [PubMed: 24499181]
21. Gavin AC, et al. Proteome survey reveals modularity of the yeast cell machinery. Nature. 2006; 440:631–636. nature04532 [pii]. DOI: 10.1038/nature04532 [PubMed: 16429126]
22. Krogan NJ, et al. High-definition macromolecular composition of yeast RNA-processing complexes. Mol Cell. 2004; 13:225–239. S1097276504000036 [pii]. [PubMed: 14759368]
23. Kozak M. Downstream secondary structure facilitates recognition of initiator codons by eukaryotic ribosomes. Proc Natl Acad Sci U S A. 1990; 87:8301–8305. [PubMed: 2236042]
24. Gao Z, et al. Coupling between the DEAD-box RNA helicases Ded1p and eIF4A. Elife. 2016; 5 [pii].
25. Hilliker A, Gao Z, Jankowsky E, Parker R. The DEAD-box protein Ded1 modulates translation by the formation and resolution of an eIF4F-mRNA complex. Mol Cell. 2011; 43:962–972. [pii]. DOI: 10.1016/j.molcel.2011.08.008S1097-2765(11)00585-5 [PubMed: 21925384]
26. Putnam AA, Jankowsky E. AMP sensing by DEAD-box RNA helicases. J Mol Biol. 2013; 425:3839–3845. [pii]. DOI: 10.1016/j.jmb.2013.05.006S0022-2836(13)00305-7 [PubMed: 23702290]
27. Jain S, et al. ATPase-Modulated Stress Granules Contain a Diverse Proteome and Substructure. Cell. 2016; 164:487–498. DOI: 10.1016/j.cell.2015.12.038 [PubMed: 26777405]
28. Andrews SJ, Rothnagel JA. Emerging evidence for functional peptides encoded by short open reading frames. Nat Rev Genet. 2014; 15:193–204. [pii]. DOI: 10.1038/nrg3520nrg3520 [PubMed: 24514441]
29. Tang HL, et al. Translation of a yeast mitochondrial tRNA synthetase initiated at redundant non-AUG codons. J Biol Chem. 2004; 279:49656–49663. DOI: 10.1074/jbc.M408081200 [PubMed: 15358761]
30. Aylett CH, Boehringer D, Erzberger JP, Schaefer T, Ban N. Structure of a yeast 40S-eIF1-eIF1A-eIF3-eIF3j initiation complex. Nat Struct Mol Biol. 2015; 22:269–271. [pii]. DOI: 10.1038/nsmb.2963nsmb.2963 [PubMed: 25664723]
31. Hu W, Sweet TJ, Chamnongpol S, Baker KE, Coller J. Co-translational mRNA decay in Saccharomyces cerevisiae. Nature. 2009; 461:225–229. [pii]. DOI: 10.1038/nature08265nature08265 [PubMed: 19701183]
32. Smith JE, et al. Translation of small open reading frames within unannotated RNA transcripts in Saccharomyces cerevisiae. Cell Rep. 2014; 7:1858–1866. [pii]. DOI: 10.1016/j.celrep.2014.05.023S2211-1247(14)00398-2 [PubMed: 24931603]
33. Goecks J, Nekrutenko A, Taylor J. Galaxy: a comprehensive approach for supporting accessible, reproducible, and transparent computational research in the life sciences. Genome Biol. 2010; 11:R86. [pii]. [PubMed: 20738864]
34. Andreev DE, et al. Translation of 5′ leaders is pervasive in genes resistant to eIF2 repression. Elife. 2015; 4:e03971. [PubMed: 25621764]
35. Matz M, et al. Amplification of cDNA ends based on template-switching effect and step-out PCR. Nucleic Acids Res. 1999; 27:1558–1560. gkc271 [pii]. [PubMed: 10037822]
36. Nagalakshmi U, et al. The transcriptional landscape of the yeast genome defined by RNA sequencing. Science. 2008; 320:1344–1349. [pii]. DOI: 10.1126/science.11584411158441 [PubMed: 18451266]
37. Konig J, et al. iCLIP reveals the function of hnRNP particles in splicing at individual nucleotide resolution. Nat Struct Mol Biol. 2010; 17:909–915. [pii]. DOI: 10.1038/nsmb.1838nsmb.1838 [PubMed: 20601959]
38. Subtelny AO, Eichhorn SW, Chen GR, Sive H, Bartel DP. Poly(A)-tail profiling reveals an embryonic switch in translational control. Nature. 2014; 508:66–71. [pii]. DOI: 10.1038/nature13007nature13007 [PubMed: 24476825]

Author Manuscript Author Manuscript Author Manuscript Author Manuscript

39. Licatalosi DD, et al. HITS-CLIP yields genome-wide insights into brain alternative RNA processing. Nature. 2008; 456:464–469. [pii]. DOI: 10.1038/nature07488nature07488 [PubMed: 18978773]
40. Park D, Morris AR, Battenhouse A, Iyer VR. Simultaneous mapping of transcript ends at single-nucleotide resolution and identification of widespread promoter-associated non-coding RNA governed by TATA elements. Nucleic Acids Res. 2014; 42:3736–3749. [pii]. DOI: 10.1093/nar/gkt1366gkt1366 [PubMed: 24413663]
41. Robinson JT, et al. Integrative genomics viewer. Nat Biotechnol. 2011; 29:24–26. [pii]. DOI: 10.1038/nbt.1754nbt.1754 [PubMed: 21221095]
42. Pettersen EF, et al. UCSF Chimera--a visualization system for exploratory research and analysis. J Comput Chem. 2004; 25:1605–1612. DOI: 10.1002/jcc.20084 [PubMed: 15264254]
43. Eden E, Navon R, Steinfeld I, Lipson D, Yakhini Z. GOrilla: a tool for discovery and visualization of enriched GO terms in ranked gene lists. BMC Bioinformatics. 2009; 10:48. [pii]. [PubMed: 19192299]
44. Gruber AR, Bernhart SH, Lorenz R. The ViennaRNA web services. Methods Mol Biol. 2015; 1269:307–326. DOI: 10.1007/978-1-4939-2291-8_19 [PubMed: 25577387]
45. Team, R. RStudio: Integrated Development for R. RStudio, Inc; Boston, MA: 2015. http://www.rstudio.com/
46. Team, R. C. R: A language and environment for statistical computing. R Foundation for Statistical Computing; Vienna, Austria: 2013. http://www.R-project.org
47. SGD, D. http://www.yeastgenome.org
48. Benjamini Y, Hochberg Y. Controlling the False Discovery Rate: A Practical and Powerful Approach to Multiple Testing. J Royal Statist Soc. 1995; 57:289– 300.
49. Miyasaka H. The positive relationship between codon usage bias and translation initiation AUG context in Saccharomyces cerevisiae. Yeast. 1999; 15:633–637. [pii]. DOI: 10.1002/(SICI)1097-0061(19990615)15:8<633::AID-YEA407>3.0.CO;2-O [PubMed: 10392441]
50. Nielsen KH, et al. Synergistic activation of eIF4A by eIF4B and eIF4G. Nucleic Acids Res. 2011; 39:2678–2689. [pii]. DOI: 10.1093/nar/gkq1206gkq1206 [PubMed: 21113024]
51. Floor SN, Condon KJ, Sharma D, Jankowsky E, Doudna JA. Autoinhibitory Interdomain Interactions and Subfamily-specific Extensions Redefine the Catalytic Core of the Human DEAD-box Protein DDX3. J Biol Chem. 2016; 291:2412–2421. [pii]. DOI: 10.1074/jbc.M115.700625M115.700625 [PubMed: 26598523]
52. Siepel A, et al. Evolutionarily conserved elements in vertebrate, insect, worm, and yeast genomes. Genome Res. 2005; 15:1034–1050. gr.3715005 [pii]. DOI: 10.1101/gr.3715005 [PubMed: 16024819]

Author Manuscript Author Manuscript Author Manuscript Author Manuscript

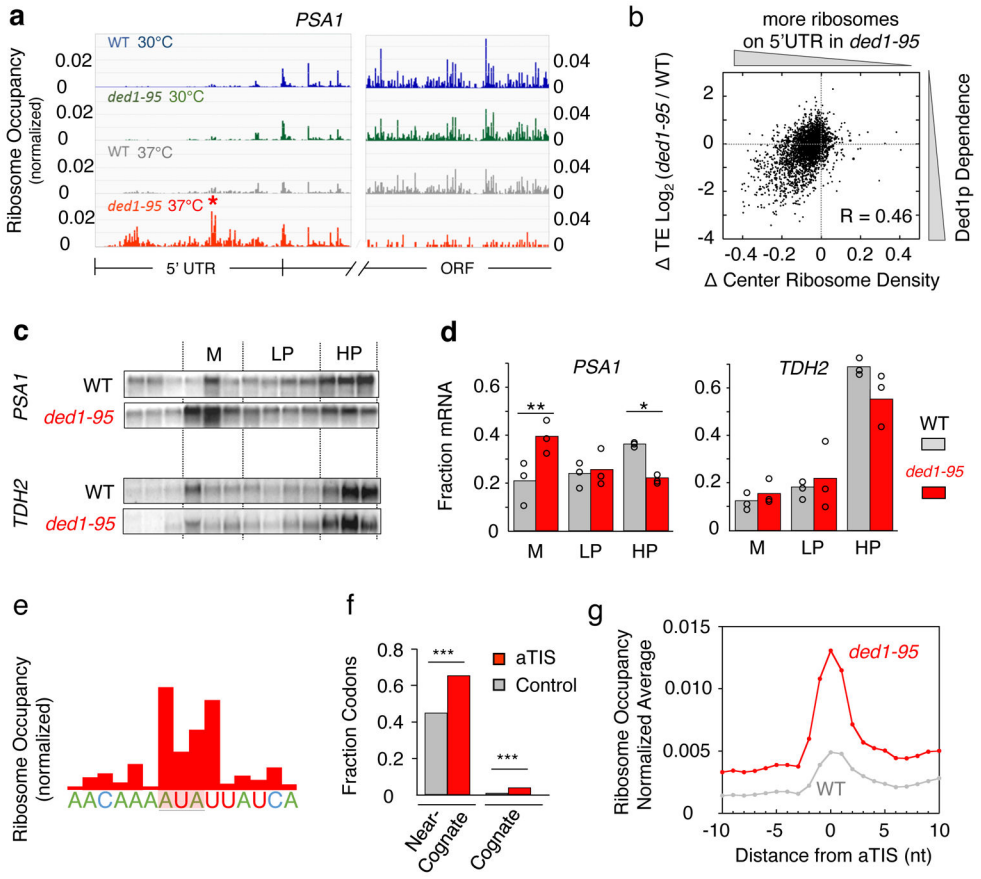

Figure 1. Defects in Ded1p activate alternative translation initiation sites

a, Ribosome profiling tracks of the 5′UTR of *PSA1* mRNA for WT *DED1* and *ded1-95*, before and 5 min after temperature shift. Bars mark the ribosome P-site, the star an alternative translation initiation site. Similar results were obtained in two independent experiments for each dataset.

b, Correlation between change in translational efficiency (ΔTE) and change in the center of ribosome density of WT *DED1,* compared to *ded1-95* (N = 2,837, 5 min, 37°C, (R: Pearson correlation coefficient).

c, Representative RNA blots of *PSA1* ($\log_2\Delta TE_{PSA1} = -2.1$) and *TDH2* ($\log_2\Delta TE_{TDH2} = 0.7$) after polysome fractionation for WT *DED1* and *ded1-95*, 5 min after temperature shift. M: 80S monosomes, LP: light polysomes, HP heavy polysomes. Similar results were obtained in three independent experiments.

d, Quantification of *PSA1* and *TDH2* RNA blots. Bars indicate the fraction of the mRNA in monosomes (M), light polysomes (LP), and heavy polysomes (HP) (* p = 0.036; **p = 0.004, two-tailed t-test).

e, Representative ribosome profiling track for a segment in the 5′UTR of *PSA1* (indicated by star in panel (**a**) in *ded1-95* (5 min, 37°C). The near-cognate initiation codon is highlighted. Similar results were obtained two independent experiments

f, Fraction of near-cognate and cognate initiation codons at sites with marked ribosome accumulation (red bars, aTISs, N = 396), and at randomly chosen control positions (grey) in 5′UTRs in *ded1-95*. (*** - statistical significance of the differences between WT *DED1* and

Author Manuscript Author Manuscript Author Manuscript Author Manuscript

ded1-95 (two-tailed t-test) for near-cognate codons: p = 1.1e-4, for cognate codons: p = 3.1e-5.)

k, Mean ribosome occupancy 10 nt 3′ and 5′ of high confidence aTIS on 5′UTRs (moving average: ± 1nt) for *ded1-95* (red) and WT *DED1* (5 min, 37°C).

Author Manuscript Author Manuscript Author Manuscript Author Manuscript

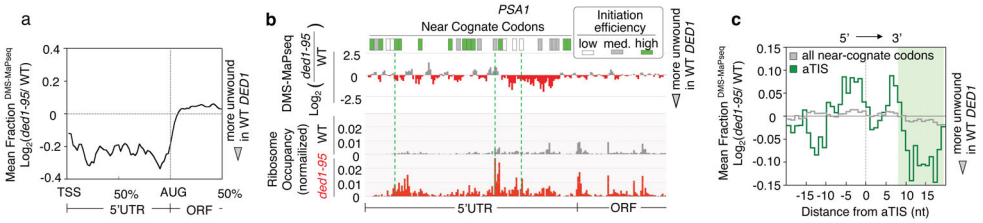

Figure 2. mRNA structure unwinding by Ded1p and aTIS activation

a, Metagene profile of mRNA unwinding by Ded1p on 5′UTRs and the 5′ moiety of ORFs (moving average: ± 1nt). Similar results were obtained in two independent experiments.

b, Representative differential DMS-MaPseq track for the 5′UTR of the *PSA1* mRNA (upper track, mRNA regions unwound in WT *DED1*marked by red bars, the more negative the value, the stronger the unwinding). Similar results were obtained in two independent experiments. For comparison, ribosome profiling traces of the 5′UTR of *PSA1* mRNA for WT *DED1* and *ded1-95* are shown. Near-cognate codons are color-coded according to their initiation efficiency, as indicated. Green lines mark activated aTISs.

c, Localization of unwound mRNA structure 3′ of activated aTISs. Enrichment of differential DMS-MaPseq counts. Negative values indicate unwound mRNA regions in WT *DED1* within 20 nt of high stringency aTISs (N = 274), compared to all other near-cognate codons (N = 60,666; excluding aTIS). The shaded area marks a significant difference in 2° RNA structure between the regions downstream of an aTIS and downstream of any near cognate codon (p = 0.00004, two-tailed t-test). The dashed line marks the 5′ nucleotide of the aTISs or the near- cognate codon.

Author Manuscript Author Manuscript Author Manuscript Author Manuscript

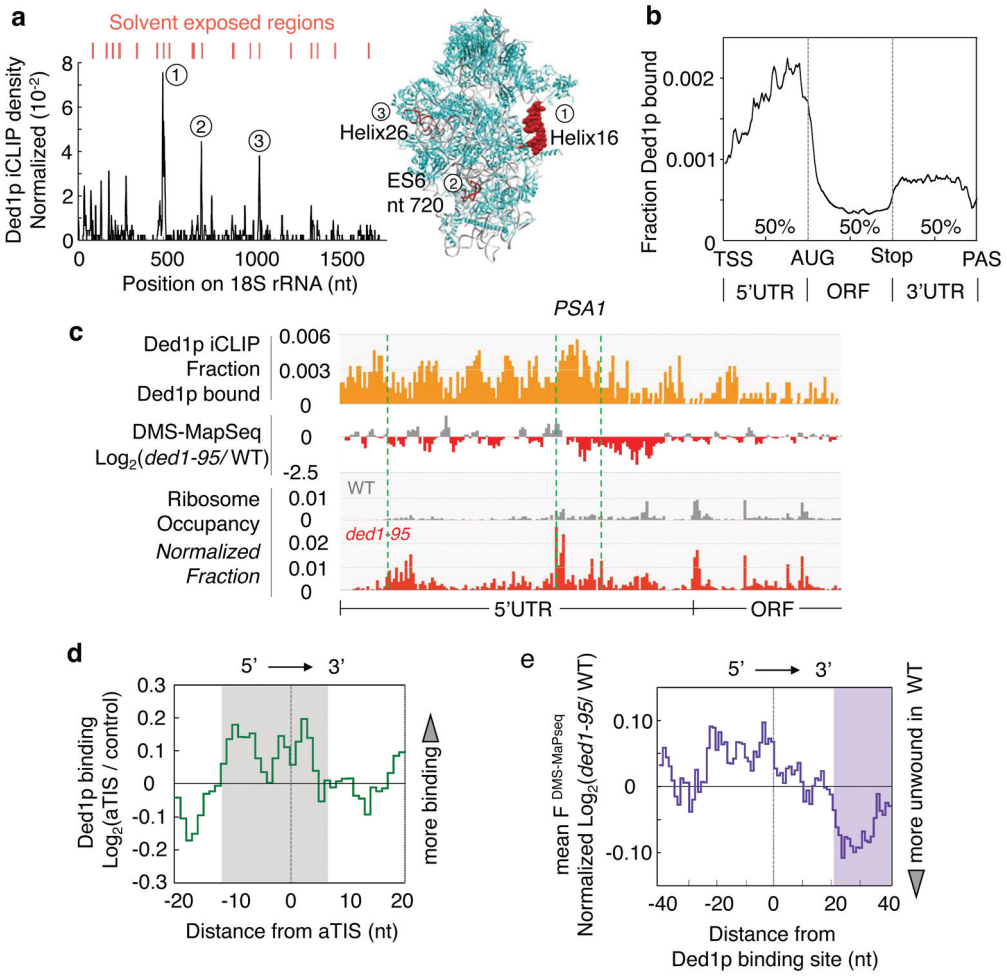

Figure 3. Ded1p crosslinking to the 40S ribosomal subunit and to mRNAs

a, Fraction of iCLIP RT stops on 18S rRNA (moving average: ± 2nt, values represent the average from two independent experiments). Numbers denote predominant crosslinking sites. Position of the three predominant Ded1p crosslinking sites (red) in the crystal structure of the 40S ribosomal subunit [30] (RNA: grey, ribosomal proteins: cyan, Ded1p crosslink sites: red, ES6: Extension segment 6).

b, Metagene profile of Ded1p association to mRNAs, calculated from two independent iCLIP experiments (moving average: ± 1nt; TSS, transcription start site; AUG, translation start site; Stop, translation stop site; PAS, polyadenylation site).

c, Ded1p crosslinking to the 5′UTR of the *PSA1* mRNA (top trace: fraction of RT-stops per nt, normalized to transcript). For comparison, differential DMS-MapSeq and ribosome profiling tracks of the 5′UTR of *PSA1* mRNA for WT *DED1* and *ded1-95* are shown (5 min, 37°C). Similar results were obtained in two independent experiments.

d, Enrichment of Ded1p crosslinking within 20 nt of aTISs (N = 274) normalized to the background distribution of Ded1p binding (moving average: ± 1nt, RT stops normalized for each mRNA). The dashed line marks the aTIS position. The shaded area marks a significant difference in Ded1p binding between the regions in vicinity of an aTIS and in vicinity of a random position within the same 5′UTR (p = 0.013, two-tailed t-test).

Author Manuscript Author Manuscript Author Manuscript Author Manuscript

e, Enrichment of differential DMS-MaPseq counts (Fig. 2c) within 40 nt of Ded1p binding sites (N = 178, high stringency aTIS) on 5′UTRs. The shaded area marks a significant difference in RNA structure between the regions downstream of a Ded1p binding site and downstream of a random position within the same 5′UTR ($p = 0.008$, two-tailed t-test).

Author Manuscript Author Manuscript Author Manuscript Author Manuscript

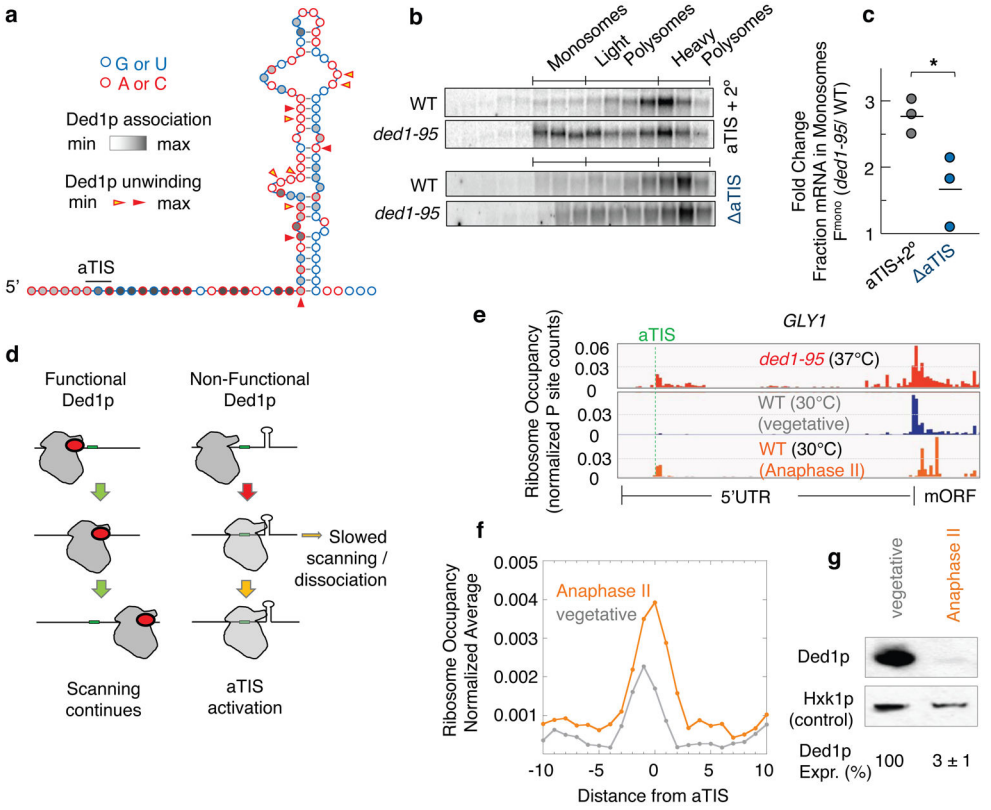

Figure 4. Ded1p function on 5′UTRs

a, DMS-MapSeq constrained secondary structure model of a fragment of the PSA1 mRNA 5′UTR. The aTIS is marked by a line. Shading indicates Ded1p crosslinking (iCLIP). Triangles indicate unwinding (DMS-MapSeq) for each nucleotide (log_2 ratio of normalized DMS-MapSeq counts of WT/*ded1-95* in two categories); yellow triangles: 0.35 - 0.7 (moderately unwound), and red triangles: > 0.7 (strongly unwound).

b, Representative RNA blots, following sucrose gradient centrifugation for WT *DED1* and *ded1-95*, (5 min, 37°C) for constructs expressing *PSA1*-FLAG mRNA with wildtype 5′UTR (aTIS + 2º), or with a mutated aTIS (ΔaTIS). Similar results were obtained in three independent experiments.

c, Quantification of RNA blot experiments (panel **b**), indicating the fold change in the fraction of PSA1 mRNA in monosomes in *ded1-95*, compared to WT upon temperature shift. (3 independent biological replicates, the line marks the average). Statistical significance of the differences between WT and *ded1-95*: p = 0.034 (two-tailed t-test).

d, Schematic model of Ded1p function on 5′UTRs. mRNA is depicted as black line, mRNA structure as schematic hairpin, the PIC as grey shape, Ded1p as red oval, and the near cognate codon as green rectangle.

e, Ribosome occupancy tracks (5 min, 37ºC) of *ded1-95* and WT *DED1* (vegetative control and Anaphase II) for *GLY1* mRNA. aTISs are marked by dashed lines. Similar results were obtained in two (vegetative control) and four (Anaphase II) independent experiments.

f, Mean ribosome occupancy 10 nt 3′ and 5′ of high confidence aTIS on 5′UTRs (moving average: ± 1nt) for WT *DED1* (vegetative control and Anaphase II).

Author Manuscript Author Manuscript Author Manuscript Author Manuscript

g, Representative Western blot of Ded1p and Hxk1p (loading control) in vegetative cells and cells in Anaphase II. Numbers indicate the relative expression level of Ded1p from four independent experiments (Error: standard deviation).